Redox Biology 45 (2021) 102048

Contents lists available at ScienceDirect

Redox Biology

journal homepage: www.elsevier.com/locate/redox

Loss of *Selenov* predisposes mice to extra fat accumulation and attenuated energy expenditure

Ling-Li Chen [a,b,c,1], Jia-Qiang Huang [a,b,1], Yuan-Yuan Wu [a], Liang-Bing Chen [a,d], Shu-Ping Li [a], Xu Zhang [a], Sen Wu [e], Fa-Zheng Ren [a,b,**], Xin-Gen Lei [f,*]

[a] Beijing Advanced Innovation Center for Food Nutrition and Human Health, Department of Nutrition and Health, China Agricultural University, Beijing, 100083, China
[b] Key Laboratory of Precision Nutrition and Food Quality, Ministry of Education, Department of Nutrition and Health, China Agricultural University, Beijing, 100083, China
[c] College of Food Science and Engineering, Jiangxi Agricultural University, Nanchang, Jiangxi, 330045, China
[d] Life Science and Agriculture Department, Zhoukou Normal University, Zhoukou, Henan, 466001, China
[e] State Key Laboratory of Agrobiotechnology, College of Biological Sciences, China Agricultural University, Beijing, 100193, China
[f] Department of Animal Science, Cornell University, Ithaca, NY, 14853, USA

ARTICLE INFO

Keywords:
Body weight
Energy balance
High-fat diet
Lipid metabolism
O-GlcNAcylation
Selenoprotein

ABSTRACT

Selenoprotein V (SELENOV) is a new and the least conserved member of the selenoprotein family. Herein we generated *Selenov* knockout (KO) mice to determine its *in vivo* function. The KO led to 16–19% increases ($P < 0.05$) in body weight that were largely due to 54% higher ($P < 0.05$) fat mass accumulation, compared with the wild-type (WT) controls. The extra fat accumulation in the KO mice was mediated by up-regulations of genes and proteins involved in lipogenesis (*Acc*, *Fas*, *Dgat*, and *Lpl;* up by 40%–1.1-fold) and down-regulations of lipolysis (*Atgl*, *Hsl*, *Ces1d*, and *Cpt1a;* down by 36–89%) in the adipose tissues. The KO also decreased ($P < 0.05$) VO_2 consumption (14–21%), VCO_2 production (14–16%), and energy expenditure (14–23%), compared with the WT controls. SELENOV and *O*-GlcNAc transferase (OGT) exhibited a novel protein-protein interaction that explained the KO-induced decreases ($P < 0.05$) of OGT protein (15–29%), activity (33%), and function (*O*-GlcNAcylation, 10–21%) in the adipose tissues. A potential cascade of SELENOV-OGT-AMP-activated protein kinase might serve as a central mechanism to link the biochemical and molecular responses to the KO. Overall, our data revealed a novel *in vivo* function and mechanism of SELENOV as a new inhibitor of body fat accumulation, activator of energy expenditure, regulator of *O*-GlcNAcylation, and therapeutic target of such related disorders.

1. Introduction

Elevated lipogenesis, coupled with decreased lipolysis and energy expenditure, often leads to positive energy balance, excessive fat accumulation, and eventually obesity [1–3]. Selenium (Se) and Se-dependent proteins have shown important roles in body lipid and energy metabolism [4–7], despite their well-known primary functions in redox control and antioxidant defense [8,9]. Knockout (KO) or overexpression of selenoprotein genes such as *Gpx1* [10,11], *Selenop* [12], *Selenom* [13], *Dio2* [14], and *Selenot* [15] in mice induced insulin resistance and obesity. As a new and the least conserved member of the 25 mammalian selenoprotein genes, *Selenov* is expressed exclusively in placental mammals [16]. The human *Selenov* gene is located on 19q13.2 and contains 5573 base pairs (bp) with 6 exons and 5 splice variants. Its primary transcript encodes 346 amino acid residues (37 kDa) [17]. Although we reported roles of SELENOV in body Se distribution and selenogenome expression [18] and in protecting mice against pro-oxidants-induced oxidative stresses [19], only a few studies have tested *in vivo* functions of the protein [20,21]. Because abundant mRNA and protein of *Selenov* were detected in the testis of mice [17,22], SELENOV was assumed a major reproductive function [23]. However, mRNA levels of *SELENOV* in several other tissues of pigs were highly responsive to a high-fat diet, which came out as the strongest independent variable for the high-fat diet-induced obesity among the 25 selenoprotein genes in a stepwise regression analysis [24]. That correlation

* Corresponding author.
** Corresponding author. Beijing Advanced Innovation Center for Food Nutrition and Human Health, Department of Nutrition and Health, China Agricultural University, Beijing, 100083, China.
E-mail addresses: renfazheng@263.net (F.-Z. Ren), XL20@cornell.edu (X.-G. Lei).
[1] Equal contribution.

https://doi.org/10.1016/j.redox.2021.102048
Received 10 April 2021; Received in revised form 13 June 2021; Accepted 14 June 2021
Available online 17 June 2021
2213-2317/© 2021 The Authors. Published by Elsevier B.V. This is an open access article under the CC BY-NC-ND license (http://creativecommons.org/licenses/by-nc-nd/4.0/).

Abbreviations:

AMPK	AMP-activated protein kinase
ACC	acetyl-CoA carboxylase
ATGL	adipose triglyceride lipase
BAT	brown adipose tissue
CES1d	carboxylesterase 1D
CPT1a	carnitine palmitoyltransferase 1A
DGAT	diacylglycerol *O*-acyltransferase
DIO2	iodothyronine, type 2
DIO3	iodothyronine, type 3
EE	energy expenditure
EWAT	epididymis white adipose tissue
FAS	fatty acid synthase
GPX1	glutathione peroxidase-1
GPX4	glutathione peroxidase-4
H&E	haematoxylin and eosin
HBP	hexosamine biosynthesis pathway
HF	high fat
HSL	hormone-sensitive lipase
IP	immunoprecipitation
IWAT	inguinal white adipose tissue
KO	knockout
LPL	lipoproteinlipase
MS	mass spectrometric
NF	normal fat
OCR	oxygen consumption rates
O-GlcNAc	*O*-linked β-*N*-acetylglucosamine
OGT	*O*-GlcNAc transferase
p450scc	cytochrome cholesterol side-chain cleavage enzyme
pAMPK	phosphorylated AMPK
PTM	post-translational modification
PGC1α	peroxisome proliferator-activated receptor-C coactivator-1α
PPARγ	peroxisome proliferator activated receptor gamma
PRDM16	PR domain containing protein 16
Q-PCR	real-time quantitative PCR
RQ	respiratory quotient
Se	selenium
Sec	selenocysteine
SELENOM	selenoprotein M
SELENOP	selenoprotein P
SELENOT	selenoprotein T
SELENOV	selenoprotein V
TC	total cholesterol
TG	triglyceride
VCO_2	carbon dioxide consumption
VO_2	oxygen consumption
WAT	white adipose tissue
UCP1	uncoupling protein 1

underscored a potential role of SELENOV in body energy and fat metabolism.

White adipose tissue (WAT) [25] is a major site of lipogenesis and stores extra fat when lipogenesis exceeds lipolysis [26], whereas brown adipose tissue (BAT) uses fat to produce heat through uncoupled respiration (nonshivering thermogenesis) [27]. Key enzymes involved in lipogenesis include: lipoprotein lipase (LPL) [28], acetyl-CoA carboxylase (ACC) [29], fatty acid synthase (FAS) [3], diacylglycerol, and acyltransferase (DGAT) [3]. Key enzymes involved in lipolysis include: adipose triglyceride lipase (ATGL) [30] and hormone-sensitive lipase (HSL) [31]. Carnitine palmitoyl transferase-1A (CPT1A) is a rate-limiting enzyme of fatty acid oxidation [32]. Thermogenesis in BAT is mediated or affected by uncoupling protein 1 (UCP1) [27], PR domain containing protein 16 (PRDM16), peroxisome proliferator-activated receptor-C coactivator-1α (PGC1α) and peroxisome proliferator activated receptor gamma (PPARγ) [33–36]. Fat accumulation may affect serum concentrations and WAT gene expression of cytokines including *TNFα*, *IL6,* and *Mcp1* [37–39] and lipid-related hormones: leptin and adiponectin [2]. While thermogenesis is related to body metabolic rate or respiration [36], it could directly affect body surface or core temperature. Thus, it is important to find out if and how SENELOV affects all these physiological, biochemical, and molecular processes in mediating its role in lipid and energy metabolism.

AMP-activated protein kinase (AMPK) and PGC1α are gate-keeping regulators of lipid and energy metabolism in adipose tissues [40,41]. While AMPK phosphorylates many downstream proteins and changes their activities [42,43], its own activity or function can be altered by two post-translational modifications (PTM): phosphorylation by upstream protein kinases [44,45] and *O*-GlcNAcylation by *O*-GlcNAc transferase (OGT) to add *O*-linked β-*N*-acetylglucosamine (*O*-GlcNAc) moieties to selected Ser and Thr residues [46,47]. These two PTM likely affect the function of AMPK and its interaction with other proteins in nutrients-sensing and metabolism-regulating [46,48,49]. In fact, OGT was shown to enhance AMPK activity by *O*-GlcNAcylation of the protein, whereas knockdown of OGT in cultured fibroblasts inhibited phosphorylation of AMPK at T172 required for its activity [46,47]. Meanwhile, PGC1α is a master regulator of mitochondrial biogenesis and energy expenditure [50], and OGT deletion exacerbated PGC1α suppression early after myocardial infarction [51]. Intriguingly, a cysteine mutant of SELENOV was shown to interact with OGT *in vitro* and overexpressed SELENOV and OGT were co-localized in COS-7 cells [23,52]. Thus, it is appealing to explore if there are a true protein-protein interaction between SELENOV and OGT and a potential SELENOV-OGT-AMPK and (or) SELENOV-OGT- PGC1α cascade to mediate metabolic impacts of the *Selenov* KO.

Therefore, we generated the *Selenov* KO mice and fed them a normal fat (NF) or a high-fat (HF) diet to determine if and how the KO affected: 1) testis and sperm functions; 2) fat mass in adipose tissues and lipid-related cytokines and hormones; 3) body temperature, body and cellular respiration, and resilience to cold stress; 4) regulation of key genes and proteins involved in lipogenesis, lipolysis, and thermogenesis in the WAT and BAT; 5) protein-protein interactions of OGT with SELENOV and the impacts on OGT activity and function; and 6) *O*-GlcNAcylation and phosphorylation of AMPK and PGC1α. Our findings reveal a novel role and mechanism of SELENOV in lipid and energy metabolism and underscore a potential new therapeutic target for treating related disorders.

2. Materials and methods

2.1. Animal experiments

All animal experiments were carried out in accordance with the recommendations of the Guide for the Care and Use of Laboratory Animals of the National Institutes of Health. Our protocol was approved by the Animal Care and Use Committee of China Agriculture University (permit number: KY150016). Mice were caged in groups (5/cage) located in a room at 22 ± 2 °C and with a 12 h light/dark cycle, given free access to diet and water, and checked daily. Mice used for the initial characterization and subsequent experiments were males, 4-month old, and fed a control (normal fat or NF) diet unless otherwise indicated.

Generation of Selenov knockout mice: The *Selenov* KO mice were generated from the C57BL/6 background using the CRISPR/Cas9 system [18]. Two sgRNAs were designed to generate a ~3 kb deletion covering

the entire coding region of *Selenov*. Genotyping was performed using 3 PCR primers (5′-TCCCTAACTCGGGTTCCACA-3'; 5′-GGTGTTTGCCCGG ACTGAGG-AGG-3'; and 5′-TGCAAGGAGACGGGAGGAATGAGAA-3′) to amplify an 808-bp fragment from the KO allele and a 675-bp fragment present in the *Selenov* wild-type (WT) allele [18].

Initial characterization of the Selenov KO mice: Relative mRNA levels of *Selenov* in various tissues of WT mice (n = 5) and age-dependent changes (3 weeks, 3 months, and 1 year, n = 5) of its expression in the testis were determined (see below) [53]. A RNAscope kit (Advanced Cell Diagnostics, Hayward, CA, USA) was used for i*n situ* hybridizations of *Selenov* mRNA expression in the testis and epididymis WAT (EWAT) of WT and KO mice (n = 5) according to the manufacturer's instructions. Relative amounts of SELENOV in the testis of WT and KO mice (n = 3) were determined (see below) [54].

Sperm count, morphology, and vitality of WT and KO mice were determined using a computer-assisted sperm analysis [55]. Testis samples of WT and KO mice were fixed in 4% paraformaldehyde at 4 °C, dehydrated, embedded in paraffin, sectioned for haematoxylin and eosin (H&E) staining, and examined by a certified pathologist. Relative mRNA levels of 5 key genes related to biosynthesis of testosterone (*StAR*, *p*450scc, *p450c17*, *3β-HSD*, and *17β-HSD*) (n = 5) and protein levels of p450scc (n = 3) in the testis of WT and KO mice were determined (see below). Serum concentrations of testosterone (n = 7) were determined using a commercial kit (Alpco, Salem, NH, USA). Body weights of WT and KO male mice fed the control diet (NF) at ages of 4, 5, and 6 months were recorded (n = 10) after overnight (8 h) fasting.

Effects of Selenov KO and high-fat diet: Young adult KO and WT male mice (2-month old, n = 5–10/genotype by diet for each individual assays) were fed a normal-fat diet (NF, 10% calories from fat) or a high-fat diet (HF, 60% calories from fat) for 2–4 months for various metabolic, biochemical, and molecular assays. Concentrations of all nutrients except for lipid were adjusted based on the energy density to keep similar between these two diets (Supplemental Table 1). Individual body weights of mice were recorded weekly.

2.2. Physiological, biochemical, and molecular analyses of lipid and energy metabolism

Overall status of body lipid metabolism: After 4-month feeding, mice (fasted overnight, n = 10) were killed to collect blood and tissues. Several internal organs, various adipose tissues (BAT and epididymis, inguen, mesentery, and perinephric WAT), and total body fat were weighted before being snap-frozen in liquid nitrogen. Tibia lengths were measured. Whole body composition of live animals before termination (n = 5) was measured by magnetic resonance imaging (MRI) using the Small Animal Body Composition Analysis and Imaging System (MesoQMR 23-060H–I; Nuimag Corp., Shanghai, China), according to the manufacturer's instructions. Histology of EWAT sections was examined as described above for testis morphology. Serum and tissue concentrations of triglyceride (TG), total cholesterol (TC), and non-esterified fatty acids (NEFA) were determined using a commercial kit (Wako, Tokyo, Japan). Respective commercial kits were also used to determine serum concentrations of adiponectin and leptin (Crystal Chem, Downers Grove, IL, USA), interleukin 6 (IL-6) and tumor necrosis factor α (TNFα) (eBioscience, San Diego, CA, USA), and monocyte chemoattractant protein-1 (Mcp1) (BioLengend, San Diego, CA, USA).

Brown adipocyte whitening and respiration of pre-adipocytes: After 2-month feeding, mice (4-month old, n = 5) were killed to collect brown adipose tissue (BAT, scapula) for histology as described above and to isolate primary preadipocytes from IWAT to determine cellular respiration. A type II collagenase (Sigma Chemical Co., St. Louis, MO, USA) was used to isolate the primary preadipocytes [56]. Cellular oxygen consumption rates were determined using an XF^e24 Extracellular Flux Analyzer (Seahorse Biosciences, MA, USA) [57]. Preadipocytes were seeded at 4000 cells/well in an XF^e24 cell culture microplate (V7-PS), and analyzed on the following day. Oxygen consumption rate (OCR) was measured over a 3-min period, followed by 3-min mixing and 2-min waiting as previously described [19].

Body temperature, respiration, and total digestible energy intake: After 3-month feeding (during the last week of 5 months of age), body surface temperature or heat image of mice (n = 5) was acquired using an infrared camera (FLIR T420, FLIR systems AB, Sweden). Rectal temperature was recorded using a rectal probe connected to a digital thermometer (Yellow Spring Instruments, Yellow Springs, OH, USA). The probe was inserted into the anal ducts of the mice (~2 cm) when animals were awake without anesthesia. The acute cold exposure was imposed to mice housed individually in cages at 4 °C for 1 h. Thereafter, a metabolic monitoring system (Metabolic Monitoring, Harvard, MA, USA) was used to measure total physical activity, VO_2 consumption, VCO_2 production, and energy expenditure as previously described [58,59]. Mice (5-month old, n = 5) were housed individually in chambers (22 ± 2 °C, a 12-h light/dark cycle, and free access to food and water) and were acclimated for 1 d before the 48-h recording. Respiration quotient (RQ) was calculated as follows: $RQ = VCO_2/VO_2$. Diet intakes were recorded and feces were collected, and energy of the samples were determined by oxygen bomb calorimeter (IKA C6000, Werke GmbH & CO. KG, Staufen, Germany). Digestible energy (DE) was calculated using the equations: $DE=(GE_{in}–GE_{out})/F_{in}$, where DE is the digestible energy content in diets (kal/g), GE_{in} is the total gross energy intake (kal), GE_{out} is the gross energy in feces (kal), F_{in} is the total feed intake (g).

Quantitative polymerase chain reaction (Q-PCR): Relative mRNA levels of *Selenov* in various tissues (n = 5), 5 key genes related to testosterone biosynthesis (*StAR*, *p*450scc, *p450c17*, *3β-HSD*, and *17β-HSD*) (n = 5) in the testis, *TNFα*, *IL-6,* and *Mcp1* in the EWAT (n = 5), and 11 key genes involved in lipogenesis, lipolysis, and thermogenesis in the EWAT and BAT (n = 5) were determined by Q-PCR. Briefly, total mRNA was isolated (50–100 mg tissue), prepared, and detected using ABI 7500 (Applied Biosystems, Foster City, CA) as previously described [53]. Primer sequences and efficiencies are presented in Supplementary Table 2. Potential DNA contamination of the extraction was eliminated using the DNA-free kit (Ambion, Thermo Fisher Scientific, Waltham, MA, USA), and the RNA quality was verified by both agarose gel (1%) electrophoresis and spectrometry (A260/A280). The relative mRNA level of a gene of interest was defined as the concentration of that gene/the geometric mean concentration of *β-actin* and *Hprt*, where concentration = $\text{efficiency}^{\text{average Ct(contol)}-\text{average Ct(treatment)}}$ [60].

Western blot analyses: Relative protein levels of SELENOV and p450scc protein in the testis (n = 3), 11 key factors involved in lipogenesis, lipolysis, and thermogenesis in the EWAT and (or) BAT (n = 5), and OGT, AMPK, pAMPK, and PGC1α in the EWAT and BAT (n = 5) were determined by Western blot as previously described [54]. Detailed information on antibodies is presented in Supplemental Table 3. Tissue lysates were prepared in RIPA buffer containing a protease inhibitor cocktail (Solarbio, Beijing, China). Protein concentrations of the lysates were determined using a BCA protein assay kit (Thermo Fisher Scientific, Wilmington, MA, USA). After incubating with first antibody and the corresponding second antibody, the washed blot was detected using chemiluminescence (Amersham ECL™, GE Healthcare, Piscataway, NJ, USA). Relative densities of target protein bands were quantified with ImageJ and normalized with the reference protein β-actin.

2.3. Protein-protein interaction between SELENOV and O-GlcNAc transferase (OGT)

Screening for SELENOV-interacting protein by GST-SELENOV pull-down and mass spectrometry (MS): GST-SELENOV (mutation at U255) protein was produced by inserting the gene into an expression vector pET28a (Novagen, Madison, WI, USA) and expressing the plasmid in *E.* coli strain BL21. The expressed protein was purified using the GST-tag (GE Healthcare, Piscataway, NJ, USA), immobilized on glutathione sepharose beads (GE Healthcare, Piscataway, NJ, USA), and incubated with homogenate of testis (WT mice, 4-month old) for 12 h. The binding

complex was pulled down by centrifugation, eluted, and subjected to MS. Peptide mass information was obtained by using matrix-assisted laser desorption ionization time-of-flight (MALDI-TOF/TOF) MS (Autoflex II, Bruker Daltonik, Bremen, Germany). Proteins were identified using MASCOT software (Matrix Science, Boston, MA, USA) and the NCBI data base for mouse proteome to search for peptide mass finger printing and peptide sequence tagging. Candidates with more than 5 matched peptides were selected for subsequent tests.

Formation of SELENOV-OGT protein complex: DNA fragments encoding OGT (residues 21–473) and SELENOV (mutation at U255) were PCR-amplified and subcloned into pGEX-4T-2 (GE Healthcare, Piscataway, NJ, USA) and pET28a (Novagen, Madison, WI, USA) vectors, respectively. The recombinant plasmids were transformed into *E. coli* strain BL21 (DE3) cells that were grown, induced, and harvested as described previously [61]. Cell pellets were resuspended in lysis buffer (20 mM Tris, pH 8.0, 300 mM NaCl) supplemented with 0.1% (v/v) Triton X-100, 1 mM phenylmethanesulfonyl fluoride (PMSF) (Invitrogen, Carlsbad, CA, USA). After cell lysis by sonication and centrifugation at 18,300 rpm for 50 min at 4 °C, OGT and SELENOV were purified with GST and HIS affinity beads (GE Healthcare, Piscataway, NJ, USA), respectively. The purified GST-OGT protein (200 μg) was immobilized on glutathione sepharose beads (GE Healthcare, Piscataway, NJ, USA) and incubated with the purified HIS-SELENOV proteins at mole ratios of GST-OGT to HIS-SELENOV: 1:0.5, 1:1 and 1:2 at 4 °C for 1 h in a buffer of 20 mM Tris, pH 8.0, 300 mM NaCl, 2 mM β-mercaptoethanol, 1 mM phenylmethylsulfonyl fluoride (PMSF). After the beads were extensively rinsed with the same buffer to remove un- or nonspecifically-bound proteins, the eluates were analyzed by SDS-PAGE (10% gel) [54]. Meanwhile, genes of the other 4 candidate proteins (YBOX2, FXR1, CPSM, and ATPA) were also cloned into the same pGEX-4T-2 vector and expressed in *E. coli* strain BL21 (DE3). The purified AST-tag proteins (200 μg) were immobilized on glutathione sepharose beads and tested for protein complex formation with HIS-SELENOV protein.

Isothermal titration calorimetry (ITC): To illustrate thermodynamics of the SELENOV and OGT binding, we performed ITC at 25 °C on the Nano-ITC II Instruments (TA instruments, New Castle, DE, USA) as previously described [62,63]. Briefly, 10 μL of the purified GST-OGT (final concentration: 150 μM) solution was titrated into 1.43 mL of the purified HIS-SELENOV (final concentration: 10 μM) solution in the sample cell at 25 drops per 180 s. The control heat was determined by titrating the buffer into the protein sample. The corrected heat was obtained by subtracting the dilution heat. The final data were fitted using a nonlinear least square-fitting algorithm [62].

Co-immunoprecipitation of SELENOV overexpressed in HEK 293T cells by anti-OGT antibody: HEK 293 T cells were grown in DMEM supplemented with 10% fetal bovine serum at 37 °C in 5% CO_2. The full-length of mouse *Selenov* DNA fragment containing the selenocysteine insertion sequence element was inserted into an expression vector of pb-CAG-GFP [64] to construct plasmid pb-CAG-GFP-SELENOV as previously described [19]. After the plasmid was transfected into HEK 293 T cells (at 70% confluence) using a PolyJet kit (SignaGen, Rockville, MD, USA) [19] for 48 h, cells (2×10^6) were harvested and lysed to obtain 200 μL aliquot of lysates (70 μg of protein) that was incubated with 1 μg of anti-OGT antibody (Abcam, Cambridge, MA, USA) for 2 h at 4 °C with agitation. Thereafter, the protein-antibody complex was selectively adsorbed by incubation with dynabeads Protein G (Thermo Fisher Scientific, Wilmington, USA; 30 μL per sample) overnight. The beads were collected by centrifugation at 14,000×*g* for 2 min and washed four times with RIPA buffer and once with 50 mM Tris-HCl (pH 7.5). The collected beads were used for SDS-PAGE analysis and immunoblotting.

2.4. Effects of Selenov KO and(or) high-fat diet on the functional expression of OGT

Activity and protein of OGT and global protein O-GlcNAcylation: Total enzymatic activities of OGT in the EWAT of male mice fed the NF diet (4-month old, n = 5) were measured using a UDP-Glo™ Glycosyltransferase assay (Promega, Mannheim, Germany). After the WAT was homogenized in lysis buffer, a 15 μL aliquot (7.5 μg protein) was mixed with 10 μL of substrate mix onto 96-well plates (Corning, NY, USA) and incubated for 90 min. Then, 25 μL of UDP detection reagent were transferred and incubated at room temperature for 60 min before the absorbance was measured at 620 nm. Effects of the KO and HF diet on total OGT protein and global *O*-GlcNAcylated protein levels in the WAT and BAT of mice (6-month old, n = 5, 15 μg protein loaded per lane, see above) were determined [54].

Production, phosphorylation, and O-GlcNAcylation of AMPK and PGC1α: To search for downstream targets of OGT mediating the *Selenov* KO impacts on lipid and energy metabolism through a potential protein-protein interaction between SELENOV and OGT, we determined protein levels of AMPK, pAMPK, and (or) PGC1a in the WAT and BAT of male WT and KO mice fed the NF or HF diet (6-month old, n = 5) [54] (15 μg protein was loaded per lane, see above). The same assays were performed in the younger mice (4-month old) fed the NF diet to test if the KO effects preceded the body weight phenotype.

Because AMPK and PGC1α are potential substrates of OGT [46,47,65], we performed co-immunoprecipitation of EWAT and BAT homogenates from mice fed the NF diet (4-month old) by anti-O-GlcNAc antibody (Abcam, Cambridge, MA, USA). Briefly, after tissues were homogenized in lysis buffer, 200 μL aliquots of lysates (70 μg protein) were mixed with 1 μg of anti-O-GlcNAc antibody. After the pulldown by dynabeads Protein G, the collected beads were used for SDS-PAGE analysis and immunoblotting against pAMPK, AMPK, and PGC1α antibodies (see above).

2.5. Data analysis

Data from the WT and KO mice fed the NF and HF diets were analyzed using 2-way ANOVA to test main effects of genotypes and diets. Means were compared by Tukey honestly significant difference test. Data from the two genotypes of mice fed the NF (control) diet were analyzed using a Student's *t*-test. Data were expressed as mean ± SE, and statistical significance was set at $P < 0.05$. All data were analyzed using SPSS for Windows (version 13; SPSS Inc, Chicago, IL, USA).

3. Results

3.1. Knockout of Selenov enhanced body weight without effect on male reproduction

Testis expressed the highest level and brain, adipose tissues, and muscle expressed moderate to low levels of *Selenov* mRNA, respectively, among various tissues of adult male mice (4-month old) (Fig. 1A). In the testis, the *Selenov* mRNA abundance peaked at 3 months of age in comparison with that at 3 weeks or 1 year of age (Fig. 1B). Such a high expression of *Selenov* in the testis implied a potentially important role of the gene in reproduction [21,22]. To test this premise, we generated *Selenov* KO mice by deleting the entire coding region (~3 kb) (Fig. 1C). The deletion of *Selenov* gene, along with the inactivation of the gene expression and protein production, in the testis and (or) WAT were confirmed by genotyping (Fig. 1D), *in-situ* hybridization (RNAscope) (Fig. 1E), and Western blot (Fig. 1F). However, the *Selenov* KO showed no effect on sperm morphology or testicular histology (Fig. 1G), functional measures of computer-assisted sperm analysis (Supplemental Table 4), serum concentrations of testosterone, or testis gene expression and protein production involved in the testosterone biosynthesis (Supplemental Fig. 1B-D). There was only one exception that the KO mice had slightly lower ($P < 0.05$) sperm count in the testis than the WT mice (Supplemental Fig. 1A, C). Likewise, the KO mice did not exhibit apparent changes in breeding or reproduction including birth rate, litter size, or gender ratio and survival of the offspring, compared with the WT mice. However, body weights of the KO male mice were 8% and 12%

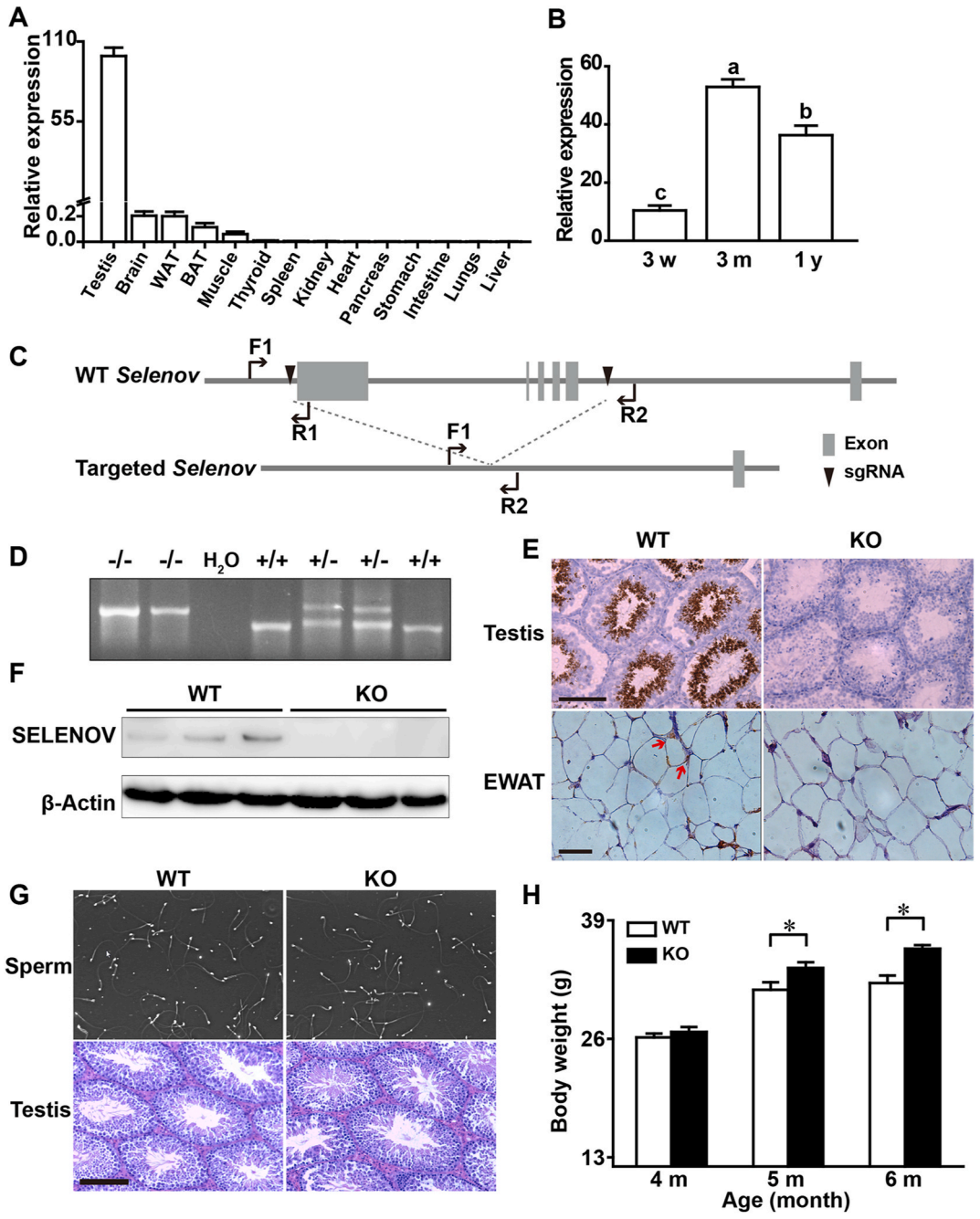

Fig. 1. Expression and knockout of *Selenov* and the knockout effects on reproduction and body weight of mice. All mice were male, fed a normal diet (Se-adequate), and 4-month old unless otherwise indicated. (A) Expression of *Selenov* mRNA in various tissues of WT mice (n = 5) relative to that of testis (set as 100). (B) Expression of *Selenov* mRNA in testis of male WT mice at ages of 3 months (3 m) and 1 year (1 y) relative to that at age of 3 weeks (3 w, set as 10) (n = 5, bars showing a different letter were different at $P < 0.05$). (C) CRISPR/Cas9 gene-targeting strategy for the generation of *Selenov* KO mice. Two sgRNAs (black triangles) were designed to generate a ~3 kb deletion covering the entire coding region of *Selenov*. Primers F1 and R2 amplified an 808 base-pair (bp) product in the targeted allele; primers F1 and R1 amplified a 675 bp product in the WT allele. (D) Genotyping of the *Selenov* WT (+/+) and KO (−/−) by PCR of genomic DNA: WT (+/+) had a 675 bp band, KO (−/−) had an 808 bp band, and heterozygote (±) had both bands. (E) RNAscope images (*in-situ* hybridization) showing high and low expression of *Selenov* in the testis and EWAT of WT mice, respectively (red arrows indicating the presence of *Selenov*), but no detectable expression in either tissue of the KO mice. Scale bars, 100 μm for testis and 50 μm for EWAT. The image was a representative of five sets of data. (F) Western blot analysis of SELENOV in the testis of WT and KO mice (n = 3). (G) Images of sperm (upper panel, magnification, × 8) and H&E staining of testis (bottom panel, scale bar, 100 μm) showing no apparent morphological abnormalities by the KO. The image was a representative of five sets of data. (H) Average body weights of mice at 4, 5, and 6 months of age (n = 10): *$P < 0.05$ for the body difference between the WT and KO mice. Data in (A), (B), and (H) are mean ± SE. Abbreviations: BAT, brown adipose tissue; bp, base pairs; EWAT, epididymis white adipose tissue; WAT, white adipose tissue; KO, knockout; WT, wild-type. (For interpretation of the references to color in this figure legend, the reader is referred to the Web version of this article.)

higher ($P < 0.05$) than their WT controls at 5 and 6 months of age, respectively (Fig. 1H).

3.2. Knockout of Selenov predisposed mice to extra fat accumulation

Both KO and HF diet elevated ($P < 0.05$) body weights of mice. The KO mice were heavier ($P < 0.05$) than the WT mice after 20 weeks of age, independent of the diet (NF or HF) (Fig. 2A). The genotype difference was 16% and 19% ($P < 0.05$) at the endpoint (6-month old) for the NF and HF diet groups, respectively. Both vertical and cross-sectional MRI of mice illustrated elevated fat accumulation by the KO and the HF diet (Fig. 2B). Weights of total and individual adipose tissues were enhanced ($P < 0.05$) by the KO and (or) HF diet. Compared with the WT mice, the KO mice fed the NF diet gained ($P < 0.05$) 54% more total fat, 31% more BAT, 1.4-fold more epididymis WAT (EWAT), 1.5-fold more inguen WAT, 99% more mesentery WAT, and 2.0-fold more perinephric WAT, respectively. Meanwhile, the KO mice fed the HF diet gained ($P < 0.05$) 54% more total fat, 25% more EWAT, and 1.1-fold more perinephric WAT than the WT, respectively. In contrast, other organ weights, except for liver weights and tibia lengths, were largely unaltered by the KO (Supplemental Table 5). Compared with the WT mice, the KO mice fed either NF or HF diet displayed adipocyte hypertrophy and enlarged lipid droplets in the (Fig. 2C). Serum TC concentrations were 50% and 16% higher ($P < 0.05$) in the KO mice fed NF and HF than those of the WT at the endpoint, respectively (Fig. 2D). Whereas the HF diet exerted consistent effects on the lipid profiles in the liver, kidney, and muscle, the KO exhibited variable and moderate effects on TC concentrations in the muscle, TG concentrations in the liver and muscle,

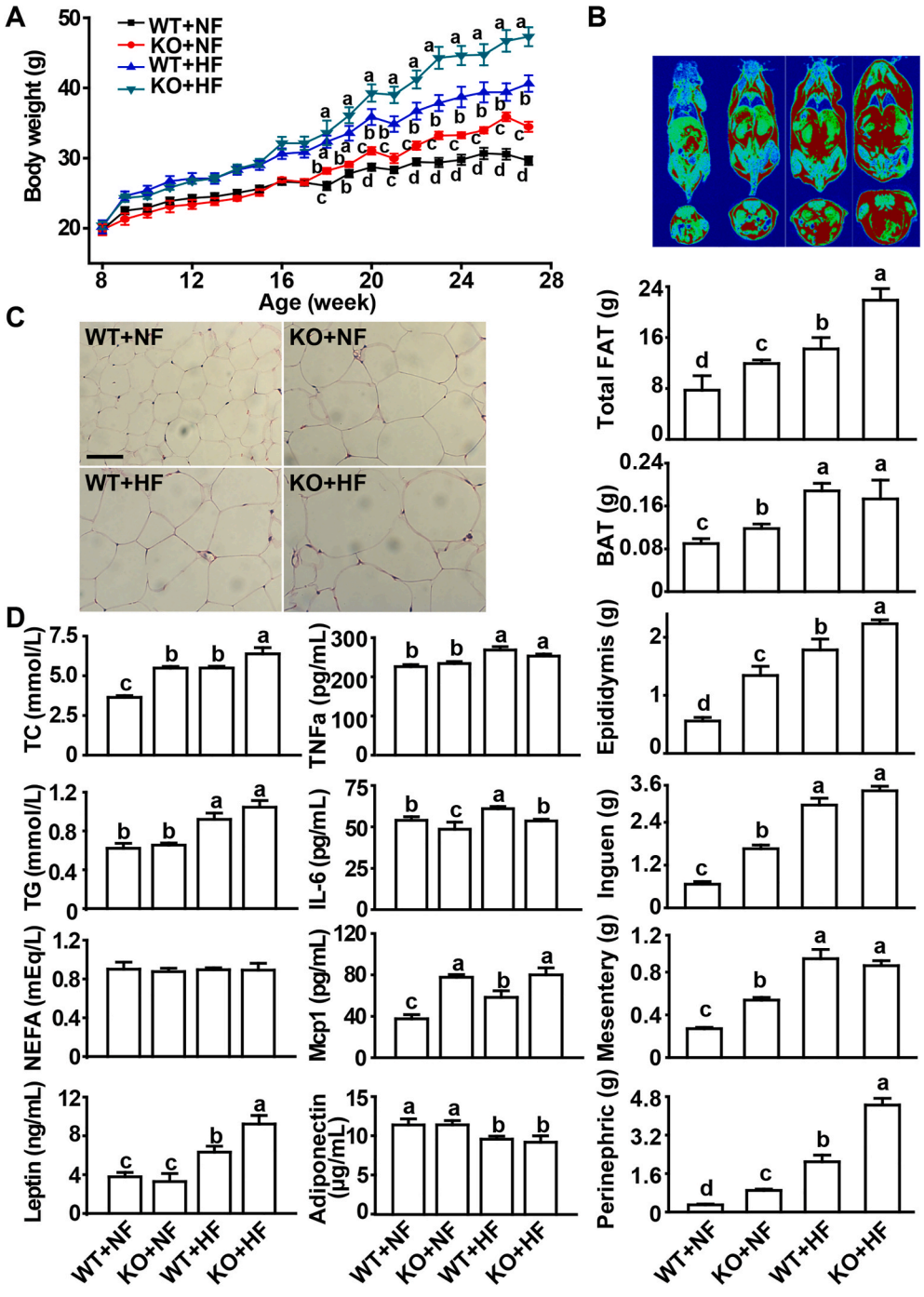

Fig. 2. Effects of *Selenov* knockout on body weight, tissue fat accumulation, adipocyte histology, and serum lipid profiles and related biomarkers in male mice fed a normal-fat (control) or a high-fat diet from 2- to 6-month old of age. (A) Body weight (n = 10). (B) Upper panel images: magnetic resonance analysis of total body fat mass. Both the vertical (top) and cross (bottom) sections showed increased fat (red color) accumulations by KO and high-fat diet. Lower bar graphs: weights of total fat and individual adipose tissues (n = 10). (C) H&E staining of paraffin-embedded EWAT sections: adipocyte hypertrophy and enlarged lipid droplets by the KO and high-fat diet, scale bar, 20 μm. The image was a representative of five sets of data. (D) Serum concentrations of TC, TG, NEFA, leptin, TNFα, IL6, Mcp1, and adiponectin (n = 6). All graphic data are mean ± SE. Means without sharing a common superscript letter are different ($P < 0.05$). Abbreviations: BAT, brown adipose tissue; EWAT, epididymis white adipose tissue; HF, high-fat diet; IL6, interleukin 6; KO, knockout; Mcp1, monocyte chemoattractant protein-1; NEFA, nonesterified fat acid; NF, normal-fat diet; TC, total cholesterol; TG, total triglyceride; TNFα, tumor necrosis factor alpha; WT, wild-type. (For interpretation of the references to color in this figure legend, the reader is referred to the Web version of this article.)

and NEFA concentrations in the liver (Supplemental Figure 2A). Serum Mcp1 concentrations in the KO mice fed the NF and HF diets were 107% and 37% higher ($P < 0.05$) than those in the WT mice, respectively. Serum TNFα concentrations were affected ($P < 0.05$) by only the HF diet, but serum IL6 concentrations were decreased ($P < 0.05$) by KO in the mice fed either diet (10–12%) (Fig. 2D). Transcript levels of *TNFα*, *IL6,* and *Mcp1* in the EWAT were up-regulated ($P < 0.05$) by KO and (or) the HF diet (Supplemental Figure 2B). Serum leptin concentrations were 46% higher ($P < 0.05$) in the KO mice fed the HF diet than those of the WT mice (Fig. 2D).

3.3. Knockout of Selenov attenuated body energy expenditure and basal metabolism

Neither KO nor the HF diet affected total dietary digestible energy intakes of mice (Fig. 3A). Infrared thermal images indicated that the KO mice were manifested with lower body surface temperature, especially in the interscapular region (black arrow) than the WT mice (Fig. 3B), as shown by decreased white color areas on the image. On the temperature indication scale, the white color represented a temperature of 32 °C and above, whereas the red/yellow color represented a temperature of 28 °C–30 °C. Average core (rectal) body temperature was 0.6 °C lower ($P < 0.05$) in the KO mice than the WT mice fed the HF diet at an ambient temperature of 22 °C (Fig. 3C). After an acute cold exposure (4 °C) for 1 h, the KO mice fed the NF diet had 0.2 °C lower ($P < 0.05$) average core temperature than the WT mice. The HF diet decreased ($P < 0.05$) the average core temperature within each genotype (Fig. 3C). Compared with the WT mice, the KO mice lost the characteristic morphology and exhibited elevated whitening in the BAT (Fig. 3D).

Total physical activities of mice over the 48-h recording period were not affected by KO, but were decreased ($P < 0.05$) by the HF diet (Fig. 3E). Total VO_2 consumptions were decreased ($P < 0.05$) by KO (14–21%) and the HF diet (15–20%). Total VCO_2 production were decreased ($P < 0.05$) by KO (16% or 14%) and the HF diet (33% or 32%). Consequently, similar genotype differences in VO_2 consumption and VCO_2 production led to similar RQ between the WT and KO mice

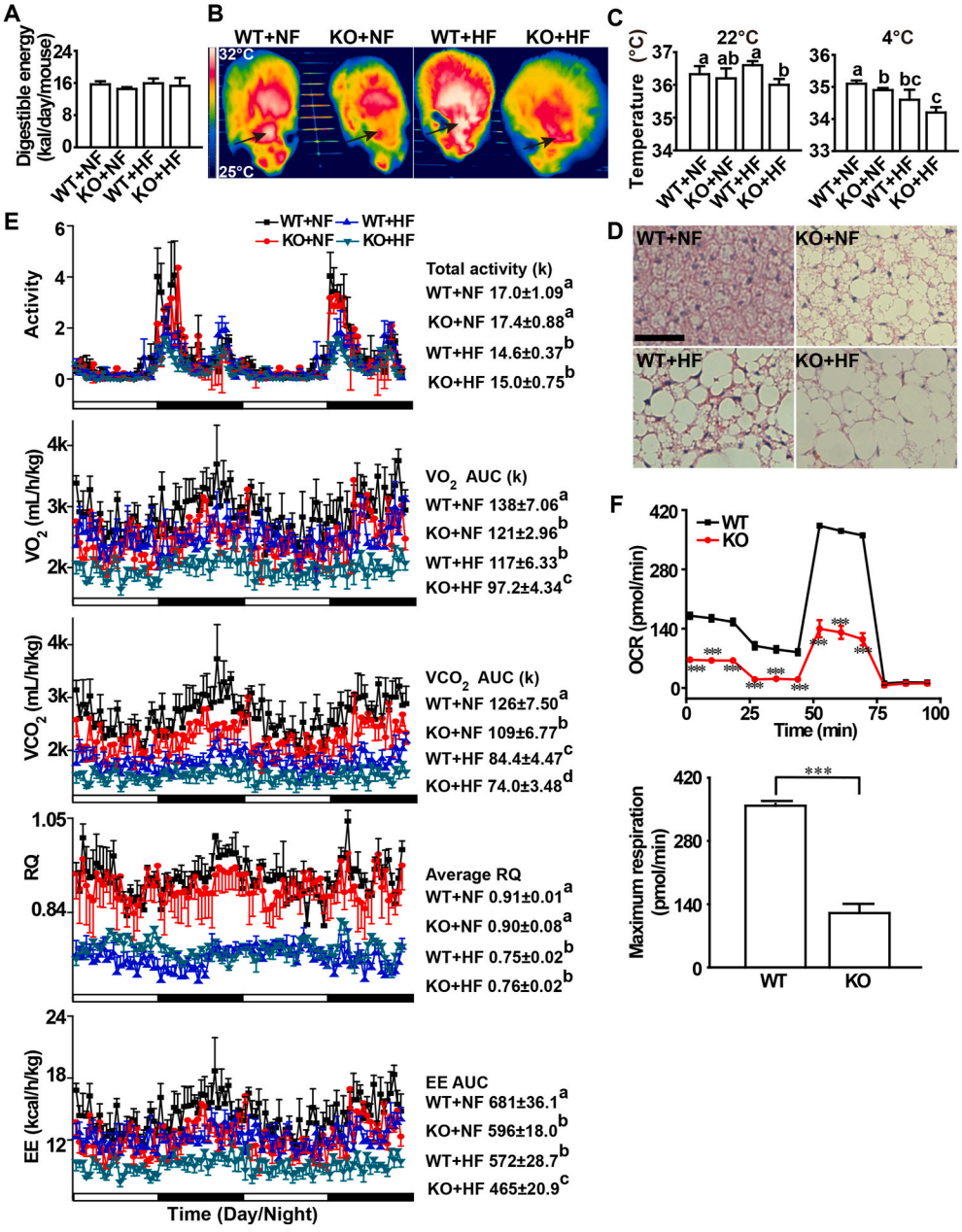

Fig. 3. Effects of *Selenov* knockout on total digestible energy intake, body surface and core temperatures, whitening of brown adipocytes, and respiration of male mice fed a normal-fat or a high-fat diet from 2- to 5-month old of age. (A) Total digestible energy intake (n = 5). (B) Representative (n = 5) infrared thermal images of body surface temperature by color coding. The images were displayed using the rainbow high contrast color palette in the FLIR Research IR112 program using a linear temperature display between 25 °C and 32 °C. The shrinking or loss of white color, especially in the interscapular region (black arrow), indicated that the KO male mice had attenuated body surface heat dissipation. (C) Average core temperature (measured with a rectal probe connected to a digital thermometer) of mice at room temperature (upper, 22 °C) or after an acute cold exposure (lower, 4 °C) for 1 h. (D) Representative image (n = 5) of H&E staining of brown adipose tissue showing loss of characteristic morphology and elevated whitening of brow adipocytes, scale bar, 20 μm. (E) Total activity, VO_2 consumption, VCO_2 production, RQ, and EE of mice (5-month old) over a 48-h period (n = 5). (F) Cellular respiration of primary pre-adipocytes of mice fed the normal diet (4-month old, n = 5). There was a sharp decline in cellular total respiration ability and maximum respiration in KO cells. All graphic data are mean ± SE. Means without sharing a common superscript letter are different ($P < 0.05$). In (F), ***$P < 0.001$ between WT and KO. Abbreviations: BAT, brown adipose tissue; EE, energy expenditure; HF, high-fat diet; KO, knockout; NF, normal-fat diet; OCR, oxygen consumption rate; RQ, respiratory quotient; WT, wild-type. (For interpretation of the references to color in this figure legend, the reader is referred to the Web version of this article.)

(Fig. 3E). Meanwhile, the HF diet shifted ($P < 0.05$) the RQ from 0.91 (carbohydrate-based energy) to 0.76 (lipid-based energy). Total energy expenditures (EE) were decreased ($P < 0.05$) by KO (14–23%) and the HF diet (16–22%). To test if the KO effect on energy metabolism preceded the appearance of body weight phenotype, we measured cellular respiration of primary preadipocytes isolated from 4-month old mice fed the NF diet. The KO decreased ($P < 0.05$) the maximum oxygen consumption rate (OCR) by 66% in those cells compared with the controls (Fig. 3F).

3.4. Knockout of Selenov stimulated lipid anabolism over catabolism in the adipose tissues

Gene transcript levels of key lipogenesis enzymes (*Acc*, *Fas*, *Dgat*, and *Lpl*) were upregulated ($P < 0.05$) by 40% to 1.1-fold in the EWAT of KO mice fed the NF diet compared with those in the WT mice (Fig. 4A). In contrast, gene transcript levels of key enzymes involved in lipolysis and fatty acid oxidation (*Atgl*, *Ces1d*, and *Cpt1a*) were downregulated ($P < 0.05$) by 36–89% in the EWAT of KO mice fed the NF diet than the WT mice. Such effects of the KO on these gene transcripts in the EWAT seemed to be attenuated or lost in mice fed the HF diet except for *Lpl* and *Atgl*. The KO elevated ($P < 0.05$) transcript level of *Hsl* in the WAT by 53% in the mice fed the NF diet, but decreased ($P < 0.05$) that by 17% in the mice fed the HF diet. The KO and (or) the HF diet elevated ($P < 0.05$) protein levels of ACC (up by 80% to 2.6-fold), FAS (up by 70–90%), HSL (up by 20% to 1-fold), but decreased ($P < 0.05$) protein levels of pACC (down by 76–88%), ATGL (down by 49–67%), and pHSL (down by 35–82%) in the EWAT (Fig. 4B).

In the BAT of mice fed either diet, the KO decreased ($P < 0.05$) transcript levels of *Cpt1a*, *Prdm16*, *Pparγ*, and *Pgc1α* by 22–41% (Fig. 4C). Compared with the NF diet, the HF diet decreased transcript levels of *Prdm16* by 41% and elevated ($P < 0.05$) those of *Pparγ* and *Pgc1α* by 20% and 1.2-fold, respectively, in the BAT of WT mice. The KO and (or) the HF diet decreased ($P < 0.05$) protein levels of CPT1A, UCP1 by 34–52% in the BAT of mice. In addition, PPARγ protein was decreased ($P < 0.05$) by the HF diet in the BAT of WT mice (Fig. 4D, Supplemental Table 6).

3.5. Knockout of Selenov decreased OGT protein, activity, and function in the adipose tissues

The GST-SELENOV pull-down and MS screening helped identify 69 candidate proteins potentially binding to SELENOV from the testis homogenates of the WT mice. Among these candidates, 9 proteins had more than 5 and OGT had the highest number of matched peptides (Supplemental Table 7). The subsequent protein binding complex formation assay indicated that only GST-OGT (Fig. 5A), but not other proteins (Supplemental Fig. 3A, B, C, D), could bind and pull-down HIS-SELENOV. It seemed that a ratio of 1:0.5 for OGT and SELENOV led to the strongest complex formation (darkest band of SELENOV).

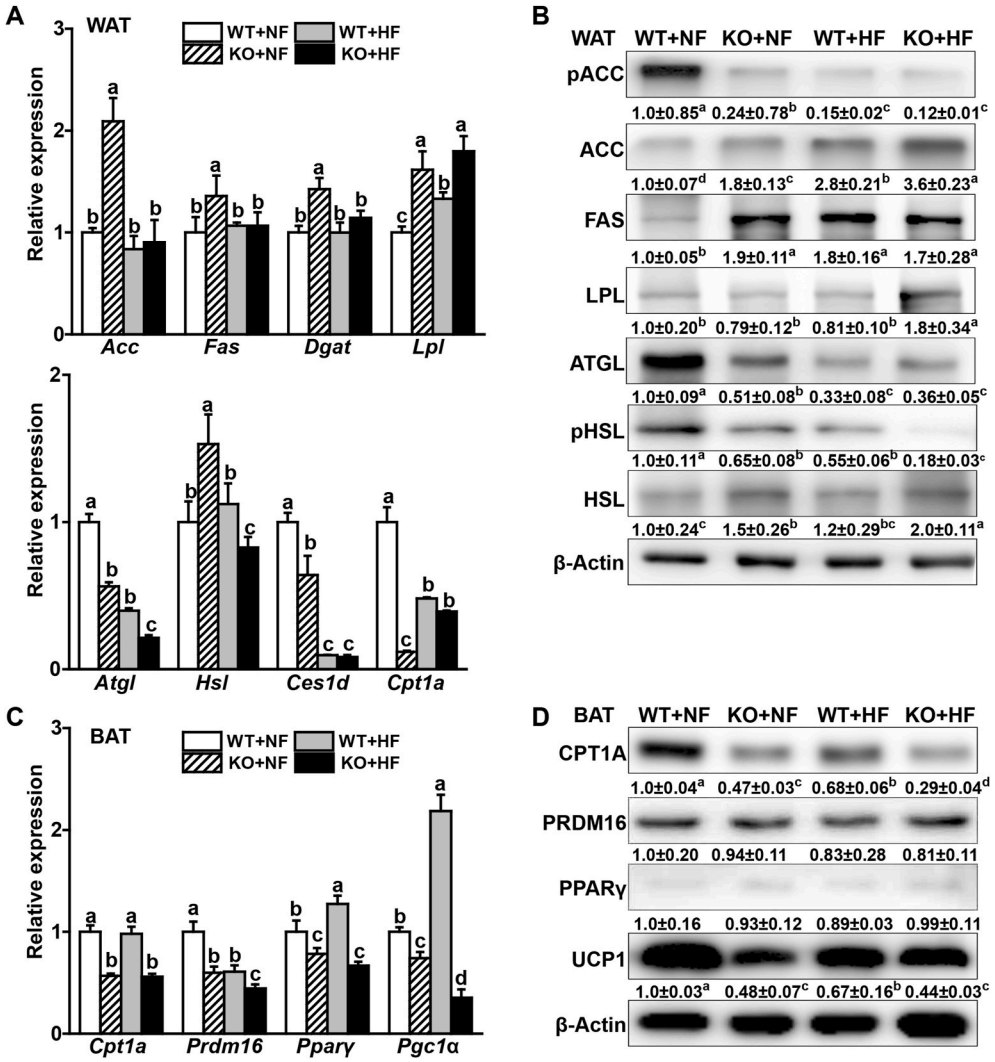

Fig. 4. Effects of *Selenov* knockout on functional expression of key regulators of lipogenesis, lipolysis, and thermogenesis in white and brown adipose tissues of male mice fed a normal-fat or a high-fat diet from 2- to 6-month old of age. (A) Relative mRNA levels of lipogenesis (upper panel) and lipolysis (lower panel) genes in the WAT (n = 5). (B) Representative image (n = 3) of Western blot analysis of lipogenesis and lipolysis-related proteins in the WAT. Values below individual bands are means of relative density of three independent replicates. (C) Relative mRNA levels of thermogenesis-related genes in the BAT (n = 5). (D) Representative image (n = 3) of Western blot analysis of thermogenesis-related proteins in the BAT. Values below individual bands are means of relative density of three independent replicates. All data are mean ± SE. Means without sharing a common superscript letter are different ($P < 0.05$). Abbreviations: *Acc*, acetyl-CoA carboxylase; *Atgl*, adipose triglyceride lipase; *Ces1d*, carboxylesterase 1D; *Cpt1a*, carnitine palmitoyltransferase 1A; *Dgat*, diacylglycerol *O*-acyltransferase; *Fas*, fatty acid synthase; HF, high-fat diet; *Hsl*, hormone-sensitive lipase; KO, knockout; *Lpl*, lipoprotein lipase; NF, normal-fat diet; *Pparγ*, peroxisome proliferator activated receptor gamma; *Prdm16*, PR domain containing protein 16; *Ucp1*, uncoupling protein 1; WT, wild-type.

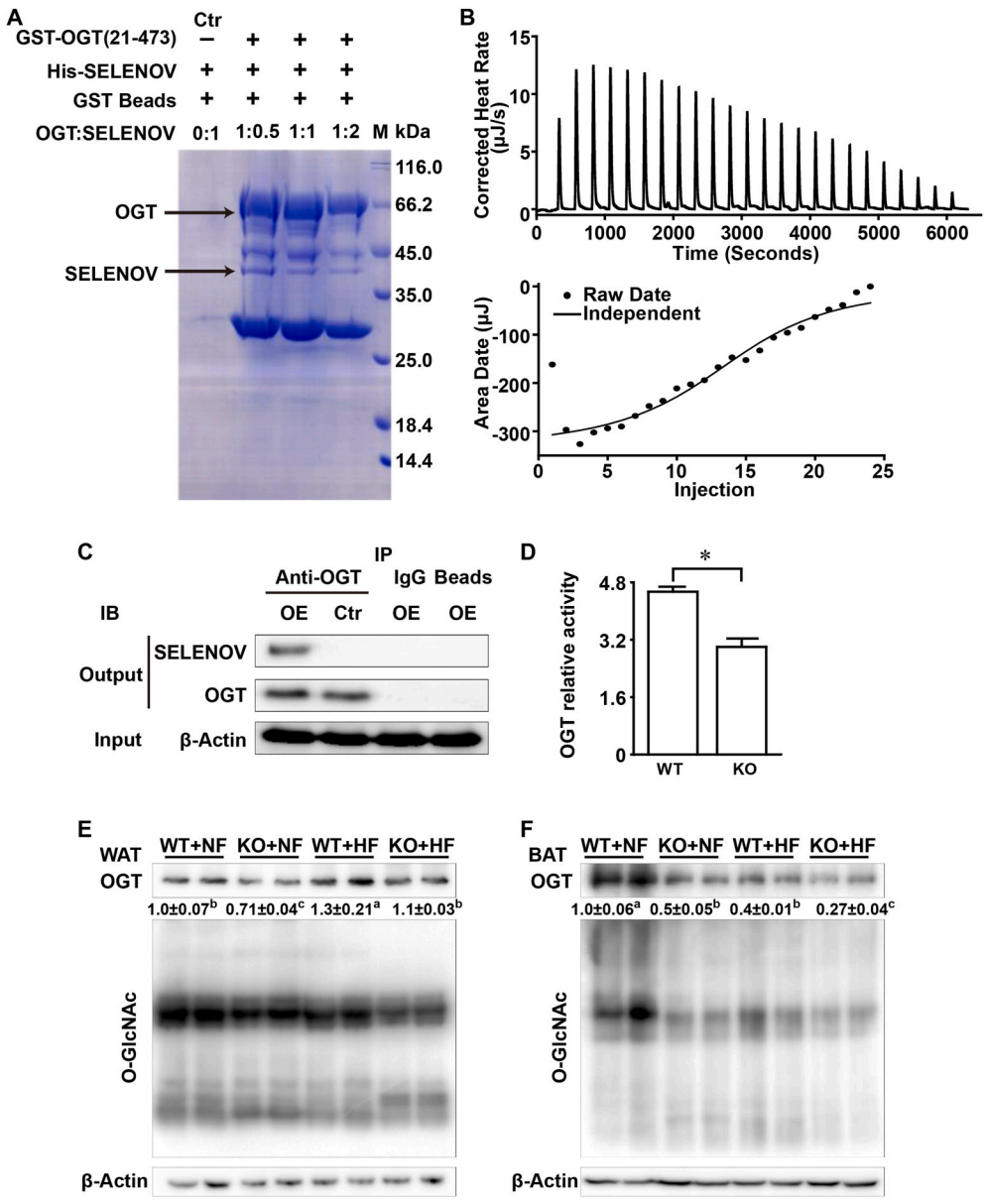

Fig. 5. Evidences for protein-protein interactions between SELENOV and *O*-GlcNAc transferase (OGT) and effects of SELENOV loss on OGT protein, activity and function in white and adipose tissues of male mice fed a normal or a high-fat diet from 2- to 6-month old of age. (A) A representative SDS-PAGE image (n = 3) showing the formation of the binding complex between the purified GST-OGT protein immobilized on glutathione sepharose beads and the purified HIS-SELENOV at different ratios. Both proteins were overexpressed in *E. coli* strain BL21. After incubation and intensive washing, the eluates were subjected to SAD-PAGE (10% gel). (B) Isothermal titration calorimetry of exothermic binding of purified GST-OGT to HIS-SELENOV protein: upper panel: corrected heat rates (μ/s) obtained for continuous injection of the OGT solution to the SELENOV solution; The positive peaks corresponded to an exothermic reaction for OGT binding to SELENOV. The heats for each injection began to decrease with an increase in the molar ratio of the OGT to SELENOV. There was little heat changes in the end, indicating that the reaction was complete. Lower panel: titration plot derived from the integrated heats of the OGT and SELENOV binding, corrected for the heat of dilution. The ITC raw date fitted well to an independent binding model, indicating that OGT could interact with SELENOV. (C) A representative image (n = 3) of immunoprecipitation of SELENOV overexpressed in HEK 293 T cells by anti-OGT antibody. Ctr: lysates of 293 T cells transfected with the control vector CAG-GFP; OE: lysates of HEK 293Tcells transfected with the *Selenov*-expressing vectors CAG-GFP-*Selenov*. (D) Enzymatic activity of OGT, measured by UDP-Glo™ Glycosyltransferase assay (Promega), in the WAT of mice fed the normal-fat diet (4-month old). Data are mean ± SE (n = 5). KO vs. WT: *P < 0.05. (E, F) Representative images (n = 3) showing relative amounts of *O*-GlcNAcylation and OGT protein in the WAT (E) and BAT (F) of mice fed a normal-fat diet or a high-fat diet from 2- to 6-month old of age. Abbreviations: BAT, brown adipose tissue; GST, glutathione-S-transferase; GST-OGT, GST tagged OGT; HF, high-fat diet; HIS-SELENOV, his tagged SELENOV; KO, knockout; NF, normal-fat diet; *O*-GlcNAc, *O*-linked β-*N*-acetylglucosamine; OGT, *O*-GlcNAc transferase; WAT, white adipose tissue; WT, wild-type. (For interpretation of the references to color in this figure legend, the reader is referred to the Web version of this article.)

Positive heat peaks (Fig. 5B, upper panel) were produced in the ITC by continuous injections of the GST-tagged OGT solution into the HIS-SELENOV solution, indicating an exothermic reaction for the binding of OGT to SELENOV. With increasing molar ratios of OGT to SELENOV, the heat peak for each injection began to attenuate, and diminished in the end when the reaction was completed. The titration plot (Fig. 5B, lower panel) derived from the integrated heats of the OGT and SELENOV binding, after being corrected for the heat of dilution, fitted well to an independent binding model to illustrate that OGT could indeed interact with SELENOV.

When lysates of HEK 293 T cells overexpressing the intact *Selenov* were incubated with the OGT antibody, the immuno-precipitated complex contained both SELENOV and OGT proteins (Fig. 5C). However, only OGT was pulled down from the control lysates. Strikingly, KO decreased ($P < 0.05$, ~40%) total OGT activity in the WAT of mice fed the NF diet (4-month old) (Fig. 5D). Levels of OGT protein in the WAT of mice (6-month old) were decreased by KO ($P < 0.05$, 15–29%), but elevated by the HF diet ($P < 0.05$, 30–55%). Global *O*-GlcNAcylated protein levels were also decreased by KO ($P < 0.05$, 10–21%) and the HF diet ($P < 0.05$, 14–24%) (Fig. 5E). Meanwhile, levels of OGT protein in the BAT of those mice were decreased by KO ($P < 0.05$, 32–50%) and the HF diet ($P < 0.05$, 46–60%). Global *O*-GlcNAcylated protein levels in the BAT of these mice were decreased by KO ($P < 0.05$, 45–56%) and the HF diet ($P < 0.05$, 36–47%) (Fig. 5F).

3.6. Knockout of Selenov suppressed O-GlcNAcylation of AMPK in the adipose tissues

The KO and (or) HF diet decreased ($P < 0.05$) phosphorylated AMPK (pAMPK) levels in the WAT and BAT of mice (6-month old) by 70–80% (Fig. 6A and B). Levels of AMPK in the WAT and BAT of mice were also decreased ($P < 0.05$) by KO and (or) HF diet, but to much less extent (20–30%). As shown in Fig. 6B, levels of PGC1α in the BAT of mice were decreased by KO ($P < 0.05$, 29–33%) and the HF diet ($P < 0.05$, 19–34%). Similar effects ($P < 0.05$) of KO on the pAMPK, AMPK, and PGC1α levels were detected in the WAT (20–82% decreases) and BAT (27–47% decreases) of 4-month old male mice fed the NF diet.

The KO decreased ($P < 0.05$) *O*-GlcNAcylation of both AMPK and pAMPK in the WAT (24–34%) (Fig. 6C) and BAT (34–50%) (Fig. 6D) of mice (4-month old) fed the NF diet. Notably, the KO decreased ($P < 0.05$) both phosphorylation and *O*-GlcNAcylation of AMPK in the WAT and BAT of these mice. However, the KO caused no change in *O*-GlcNAcylation of PGC1α in the BAT of mice (Fig. 6E).

4. Discussion

Our present study describes a successful inactivation of *Selenov* in mice, and reveals a moderate increase in body weight due to elevated fat mass accumulation across various adipose tissues in the KO mice. The creeped fat accumulation in the KO mice was associated with adipocyte hypertrophy and enlarged lipid droplets in the WAT, lost characteristic morphology and elevated whitening in the BAT, up-regulated gene expression of lipid-related cytokines in the WAT, and increased serum concentrations of these cytokines. Despite several variations, many of the KO effects remained similar between the NF and HF diet groups. Overall, we have obtained convincing evidences to unveil an important function of SELENOV in lipid metabolism, in addition to previously-demonstrated roles in regulating body Se metabolism and functional expression of selenoproteins [18] as well as in protecting against pro-oxidant-mediated oxidative stresses [19]. Our new findings not only help explain the strong correlation between the *Selenov* expression and the high-fat diet-induced obesity in pigs [24], but also qualify SELENOV to join a special group of selenoproteins involved in body energy metabolism [5]. To our best knowledge, 19 selenoprotein genes were inactivated in mice [10,12–15,66–79], and 9 of them displayed roles in

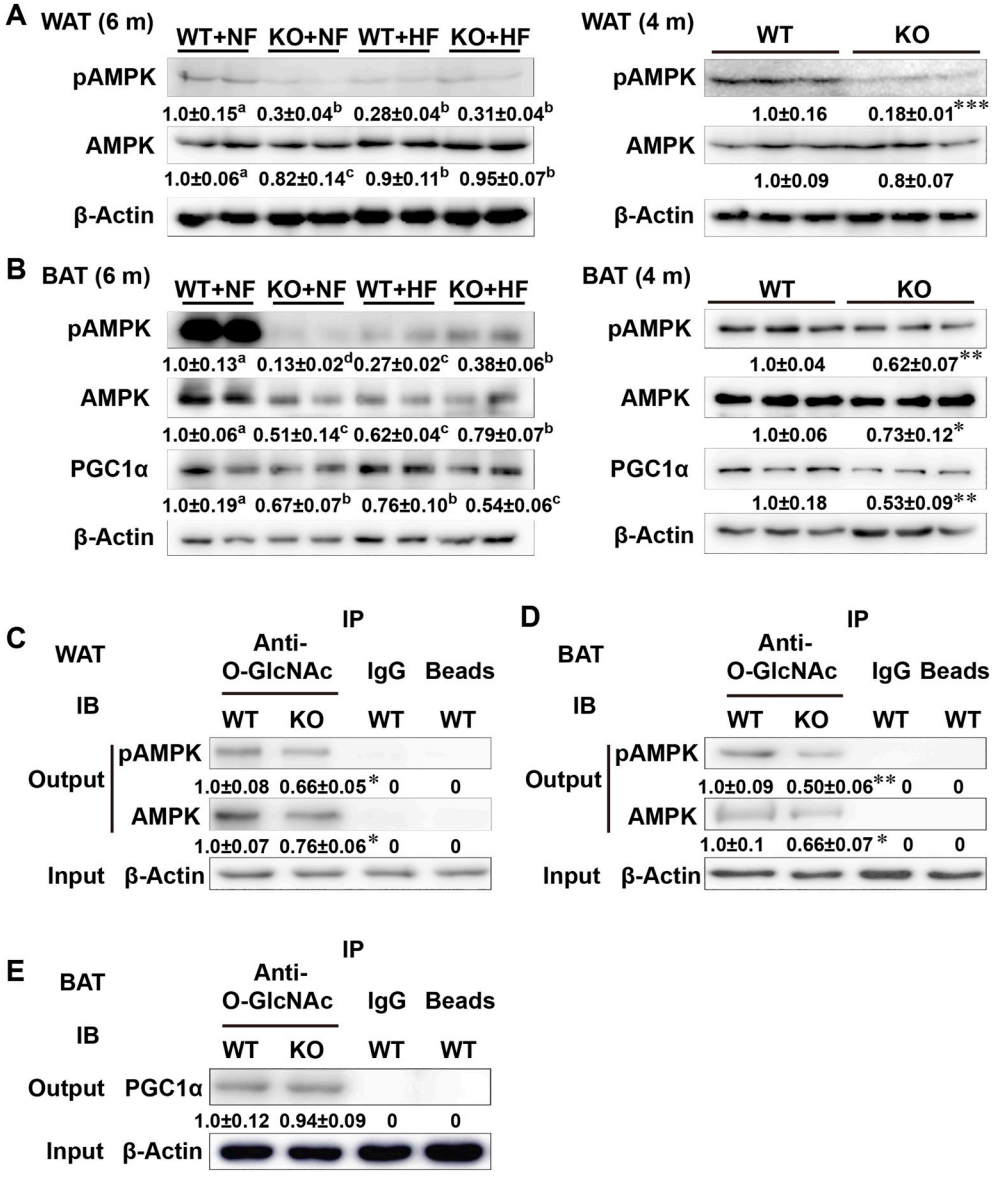

Fig. 6. Effects of *Selenov* knockout on protein production, phosphorylation, and (or) *O*-GlcNAcylation of AMPK and PGC1α in white and brown adipose tissues of male mice fed a normal-fat or a high-fat diet from 2- to 6-month old of age. (A) Representative images ($n = 5$) of immunoblots of pAMPK and AMPK in the WAT of mice (left panel: 6-month old; right panel: 4-month old and the normal diet). (B) Representative images ($n = 5$) of immunoblots of pAMPK, AMPK, and PGC1α in the BAT of mice (left panel: 6 month-old; right panel: 4-month old and the normal diet). (C, D) Representative images ($n = 3$) of immunoprecipitation of pAMPK and AMPK by anti-O-GlcNAc antibody in the WAT (C) and BAT (D) of mice (4-month old) fed the normal-fat diet. Tissue homogenates were pulled-down by anti-O-GlcNAc antibody, and immunoblotted with pAMPK and AMPK antibodies. (E) Representative images ($n = 3$) of immunoprecipitation of PGC1α by anti-O-GlcNAc antibody in the BAT of mice (4 month-old) fed the normal diet. The procedure was the same as in (C. D) except for using the PGC1α antibody for immunoblotting. Values below individual bands are means ± SE of independent replicates ($n = 3$ or 5). Values of the four treatment groups without sharing a common superscript letter are different ($P < 0.05$). Values of the two groups (WT vs. KO): *$P < 0.05$, **, $P < 0.01$, ***$P < 0.001$. Abbreviations: AMPK, AMP-activated protein kinase; BAT, brown adipose tissue; HF, high-fat diet; KO, knockout; NF, normal-fat diet; *O*-GlcNAc, *O*-linked β-*N*-acetylglucosamine; pAMPK, phosphorylated AMP-activated protein kinase; PGC1α, peroxisome proliferator-activated receptor-C coactivator-1α; WAT, white adipose tissue; WT, wild-type.

glucose, lipid, and energy metabolism [10,12–15,67–70]. Null of *Gpx1* and *Selenop* [10,12] protected mice from adiposity and/or insulin resistance, whereas deficiencies of *Dio2, Selenom, Selenot*, and *Selenof* [13–15,69] exerted opposite impacts. However, null of *Dio3* produced mixed effects on adiposity [68], insulin secretion, and glucose homeostasis [66]. Null of *Msrb1* did not aggravate the high-fat diet-induced insulin resistance [72].

A unique strength of our study is the characterization of the SELENOV role and mechanism in down-regulating energy expenditure, body temperature, respiration, and cellular OCR. The lack of genotype differences in total dietary digestible energy intakes of mice fed either the NF or HF diet underscored a mechanism beyond total energy intake or digestion for the positive energy balance to achieve the extra fat accumulation in the KO mice. Indeed, the KO mice exhibited concurrent decreases in total VO_2 consumptions and VCO_2 production, compared with the WT mice fed either diet [26]. Whereas this declined catabolism did not alter total activity of mice or shift their RQ (nutrient type as the energy source), a net decrease in EE (14–23%) in the KO mice was translated into lowered body surface heat dissipation [36], average core temperature, and (or) resilience to cold exposure, compared with the WT mice. Because BAT plays a key role in thermogenesis [27], the loss of the characteristic morphology and elevation of whitening in the BAT of the KO mice might represent a plausible mechanism for the role of SELENOV in regulating EE. Notably, the KO-mediated attenuation of EE preceded the onset of overt phenotype in the mice as shown by the decreased maximum OCR in primary preadipocytes of 4-month old mice. Similar impacts of the *Selenov* KO were shown on maximal, basal, and non-mitochondrial OCR and ATP production in primary hepatocytes [19]. In contrast, inactivation of other selenoprotein genes such as *Dio3* [68] or *Gpx1* [10] elevated EE. However, null of *Selenop* did not affect VO_2 consumption in mice [12]. Apparently, SELENOV exerted a distinctly different role in regulating thermogenesis and respiration from other selenoproteins.

The KO-induced fat accumulation was mediated by up-regulated mRNA, protein, and (or) activity levels of key lipogenesis enzymes (ACC, FAS, DGAT, and LPL) [80] and down-regulated those levels of key enzymes involved in lipolysis and fatty acid oxidation (ATGL, CES1D, and CPT1*a*) [31] in the WAT. Whereas ACC catalyzes the first step of fatty acid synthesis, FAS is the rate-limiting enzyme converting malonyl-CoA to palmitate [3]. In addition, LPL hydrolyzes triglycerides from lipoproteins and releasing fatty acids for vital tissues [81]. Meanwhile, ATGL is responsible for the initial step of lipolysis and HSL and CPT1A represent rate-limiting enzymes for the catabolism of diacylglycerol [31] and fatty acid oxidation [3], respectively. Regulations of all these genes and proteins by the KO were stronger in mice fed the NF diet than those fed the HF diet. This was because fat accumulations in the mice fed these two diets were likely derived from intrinsic metabolism (*de novo* synthesis) and extrinsic fat deposit, respectively [2]. It is very important to recognize the opposite outcome by the KO-mediated decreases in pACC (inactive) and pHSL (active) protein levels [82,83]. Likewise, the KO-induced decreases in body EE was supported by the down-regulated mRNA and (or) protein levels of key enzymes involved in thermogenesis (*Cpt1a, Prdm16, Pparγ, Pgc1α, and Ucp1)* [32–34,41] in the BAT. The HF diet exhibited similar shifts on the KO effects on these factors. It is known that BAT produces heat through uncoupled respiration (nonshivering thermogenesis) which is mediated or affected by UCP1 [27], PRDM16, PGC1α and PPARγ [35,36]. Altogether, SELENOV exerted a coordinated o regulation of these key genes and proteins involved in lipogenesis, lipolysis, and thermogenesis in the WAT and BAT. Comparatively, null of other selenoprotein genes displayed inconsistent effects on these genes. Specifically, an inactivation of *Gpx1* or *Dio3* produced no change in *Ucp1* mRNA levels in the BAT of male mice [10,68], but overexpression of *Gpx1* enhanced those of *Acc* and *Pparγ* in the liver of mice [84]. An inactivation of *Dio2* decreased *Acc* mRNA levels in the WAT of male mice, without altering those of *Hsl* and *Lpl* in the WAT or *Pgc1α* and *Ucp1* in the BAT [85].

It signifies a major advance for us to establish the protein-protein interaction between SELENOV and OGT, which helps explain the metabolic phenotype of the *Selenov* inactivation. Although previous studies showed an interaction between a cysteine mutant of SELENOV and OGT *in vitro* and a co-localization of overexpressed SELENOV and OGT in COS-7 cells [23,52], we have revised this premise substantially with multiple strong new data. We first determined the formation of SELENOV and OGT binding complex *in vitro* and validated the specificity of this interaction by screening against the binding of four other proteins selected from 69 candidates identified from the initial pull-down assay. The ability of SELENOV to bind OGT was subsequently confirmed by ITC, and the co-immuno-precipitation of the over-produced native SELENOV in HEK 293 T cells by the OGT antibody. Strikingly, we demonstrated consistent and substantial decreases in the OGT protein levels and (or) activities as well as its function: global *O*-GlcNAcylated protein levels in the adipose tissues of the KO mice compared with the WT mice. Apparently, the lack or disrupted interaction of SELENOV and OGT in the KO mice resulted in a dys-regulation or loss of the OGT protein, activity, and function [23,52]. Biomedical significance of this finding cannot be overemphasized. This is because *O*-GlcNAcylation is a highly dynamic, inducible, and reversible protein PTM, and dysfunction of this process is associated with various metabolic diseases including diabetes and obesity [86,87]. Meanwhile, OGT is the sole enzyme responsible for catalyzing the addition of *O*-GlcNAc moieties to selected serine and threonine residues of nuclear and cytosolic proteins involved in a wide variety of crucial cellular functions [88,89]. Therefore, our results reveal a new function of SELENOV, a new action mode of selenoproteins other than modulating redox and insulin signaling and protein phosphorylation [15,66,90,91] involved in nutrient metabolism, a new paradigm of PTM, and a new strategy to treat diseases associated with disrupted *O*-GlcNAcylation homeostasis [59,92–94]. Previous research has shown no other redox-related proteins to interact with OGT, let alone affecting cellular *O*-GlcNAcylation [95–97].

It is most exciting to postulate a SELENOV-OGT-AMPK cascade as a potential mechanism in mediating the fat accumulation in the KO mice. Being a gate-keeper in controlling cellular and whole body energy balances, AMPK regulates lipogenesis negatively but lipolysis positively in the adipose tissues [98,99]. Previous studies suggested a link of OGT to AMPK activity via affecting *O*-GlcNAcylation or phosphorylation of the protein in cultured fibroblasts [47,49]. From this standpoint, the KO-mediated concurrent decreases in *O*-GlcNAcylation and phosphorylation of AMPK and pAMPK in the adipose tissues were consistent with the declined OGT activity. Thus, the lowered AMPK activity, due to the suppressed two PTM, led to elevated lipogenesis and decreased lipolysis in the KO mice [47]. Importantly, it is novel to reveal SELENOV, despite only a moderate expression in the adipose tissues of mice, serving as a rather potent regulator of both *O*-GlcNAcylation and phosphorylation of AMPK and (or) pAMPK. This regulation seemed to be specific as there was no such effect of KO on PGC1α in the BAT of mice. Among the known regulators of AMPK [100,101], SELENOV represents a completely new type that links Se-dependent or antioxidant proteins to energy/lipid metabolism through a new bridge of AMPK. However, *O*-GlcNAcylation and phosphorylation of AMPK were also shown to be mutually exclusive or functionally counter-acting [48,102,103]. That notion is not supported by the KO-induced concurrent decreases of *O*-GlcNAcylation and phosphorylation of AMPK in the adipose tissues of mice in the present study. It remains to find out if the absence of SELENOV altered or de-coupled these two PTM and how the *O*-GlcNAcylation of AMPK/pAMPK influenced their phosphorylation.

It is paradoxical that the KO showed no major effect on testis and sperm morphology and function, despite the abundant expression of *Selenov* and the detectable SELENOV and OGT binding in the testis. Seemingly, SELENOV was not essential for the normal fertility or breeding under our experimental condition. Alternatively, the postulated protein-protein interaction of SELENOV and OGT in the testis might impact functions or metabolism unrelated to reproduction

directly. Another selenoprotein GPX4 is also highly expressed in testis. In contrast, a global knockout of *Gpx4* caused embryonic lethality [104], and a targeted deletion of the gene in spermatocytes or haploinsufficiency caused infertility or subfertility in male mice [105,106]. On the other hand, *Gpx4* haploinsufficiency exacerbated glucose intolerance, dyslipidemia, and liver steatosis [107]. Ablation of *Gpx4* from AgRP neurons increased the diet-induced body weight gain and fat mass in male mice by altering locomotor activity and nutrient partitioning [67]. It seemed that GPX4 and SELENOV shared similar impacts on lipid metabolism, but not reproduction.

5. Conclusion

In the present study, we have successfully created a *Selenov* KO murine model and demonstrated an elevated body fat mass accumulation as the main phenotype. The metabolic shift was characterized by up-regulated lipogenesis and down-regulated lipolysis and energy expenditure in the adipose tissues. Multiple *in vitro* and *in vivo* evidences helped establish a unique protein-protein interaction between SELENOV and OGT. The KO decreased OGT protein, activity, and function of global protein *O*-GlcNAcylation in the adipose tissues of mice. A potential SELENOV-OGT-AMPK cascade might serve as a central mechanism to mediate the metabolic responses to the KO. Overall, our data have revealed a novel *in vivo* function and mechanism of SELENOV as a new inhibitor of body fat accumulation, activator of thermogenesis, regulator of *O*-GlcNAcylation, and therapeutic target of such related disorders.

Funding

This study was supported in part by the National Natural Science Foundation of China 32002216.

Contributions of authors

XGL: conceived and designed the research; FZR: supervised the research; LLC, JQH, YYW, LBC, SPL, XZ, SW: conducted the research and analyzed the data; LLC, JQH, and XGL: wrote the paper; XGL and F-ZR: had primary responsibility for final content; and all authors: read and approved the final manuscript.

Declaration of competing interest

The authors declare no competing interests.

Appendix A. Supplementary data

Supplementary data to this article can be found online at https://doi.org/10.1016/j.redox.2021.102048.

References

[1] G.H. Goossens, The metabolic phenotype in obesity: fat mass, body fat distribution, and adipose tissue function, Obesity Facts 10 (2017) 207–215, https://doi.org/10.1159/000471488.
[2] J.M. Rutkowski, J.H. Stern, P.E. Scherer, The cell biology of fat expansion, J. Cell Biol. 208 (2015) 501–512, https://doi.org/10.1083/jcb.201409063.
[3] C. Saponaro, M. Gaggini, F. Carli, A. Gastaldelli, The subtle balance between lipolysis and lipogenesis: a critical point in metabolic homeostasis, Nutrients 7 (2015) 9453–9474, https://doi.org/10.3390/nu7115475.
[4] X. Hu, J.D. Chandler, M.L. Orr, L. Hao, K. Liu, K. Uppal, Y.M. Go, D.P. Jones, Selenium supplementation alters hepatic energy and fatty acid metabolism in mice, J. Nutr. 148 (2018) 675–684, https://doi.org/10.1093/jn/nxy036.
[5] V.M. Labunskyy, B.C. Lee, D.E. Handy, J. Loscalzo, D.L. Hatfield, V.N. Gladyshev, Both maximal expression of selenoproteins and selenoprotein deficiency can promote development of type 2 diabetes-like phenotype in mice, Antioxidants Redox Signal. 14 (2011) 2327–2336, https://doi.org/10.1089/ars.2010.3526.
[6] C. Tang, S. Li, K. Zhang, J. Li, Y. Han, T. Zhan, Q. Zhao, X. Guo, J. Zhang, Selenium deficiency-induced redox imbalance leads to metabolic reprogramming and inflammation in the liver, Redox Biol 36 (2020) 101519, https://doi.org/10.1016/j.redox.2020.101519.
[7] K.S. Prabhu, X.G. Lei, Selenium, Advances in Nutrition 7 (2016) 415–417, https://doi.org/10.3945/an.115.010785.
[8] S.a.Z. Ibrahim, A. Kerkadi, A. Agouni, Selenium and health: an update on the situation in the middle east and north africa, Nutrients 11 (2019) 1457–1469, https://doi.org/10.3390/nu11071457.
[9] V.M. Labunskyy, D.L. Hatfield, V.N. Gladyshev, Selenoproteins: molecular pathways and physiological roles, Physiol. Rev. 94 (2014) 739–777, https://doi.org/10.1152/physrev.00039.2013.
[10] K. Loh, H. Deng, A. Fukushima, X. Cai, B. Boivin, S. Galic, C. Bruce, B.J. Shields, B. Skiba, L.M. Ooms, N. Stepto, B. Wu, C.A. Mitchell, N.K. Tonks, M.J. Watt, M. A. Febbraio, P.J. Crack, S. Andrikopoulos, T. Tiganis, Reactive oxygen species enhance insulin sensitivity, Cell Metabol. 10 (2009) 260–272, https://doi.org/10.1016/j.cmet.2009.08.009.
[11] J.P. Mcclung, C.A. Roneker, W. Mu, D.J. Lisk, P. Langlais, F. Liu, X.G. Lei, Development of insulin resistance and obesity in mice overexpressing cellular glutathione peroxidase, Proc. Natl. Acad. Sci. U.S.A. 101 (2004) 8852–8857, https://doi.org/10.1073/pnas.0308096101.
[12] H. Misu, T. Takamura, H. Takayama, H. Hayashi, N. Matsuzawa-Nagata, S. Kurita, K. Ishikura, H. Ando, Y. Takeshita, T. Ota, M. Sakurai, T. Yamashita, E. Mizukoshi, T. Yamashita, M. Honda, K.-I. Miyamoto, T. Kubota, N. Kubota, T. Kadowaki, H.-J. Kim, I.-K. Lee, Y. Minokoshi, Y. Saito, K. Takahashi, Y. Yamada, N. Takakura, S. Kaneko, A liver-derived secretory protein, selenoprotein P, causes insulin resistance, Cell Metabol. 12 (2010) 483–495, https://doi.org/10.1016/j.cmet.2010.09.015.
[13] M.W. Pitts, M.A. Reeves, A.C. Hashimoto, A. Ogawa, P. Kremer, L.A. Seale, M. J. Berry, Deletion of selenoprotein M leads to obesity without cognitive deficits, J. Biol. Chem. 288 (2013) 26121–26134, https://doi.org/10.1074/jbc.M113.471235.
[14] A. Marsili, C. Aguayo-Mazzucato, T. Chen, A. Kumar, M. Chung, E.P. Lunsford, J. W. Harney, T. Van-Tran, E. Gianetti, W. Ramadan, C. Chou, S. Bonner-Weir, P. R. Larsen, J.E. Silva, A.M. Zavacki, Mice with a targeted deletion of the type 2 deiodinase are insulin resistant and susceptible to diet induced obesity, PloS One 6 (2011), e20832, https://doi.org/10.1371/journal.pone.0020832.
[15] G. Prevost, A. Arabo, L. Jian, E. Quelennec, D. Cartier, S. Hassan, A. Falluel-Morel, Y. Tanguy, S. Gargani, I. Lihrmann, J. Kerr-Conte, H. Lefebvre, F. Pattou, Y. Anouar, The PACAP-regulated gene selenoprotein T is abundantly expressed in mouse and human betacells and its targeted inactivation impairs glucose tolerance, Endocrinology 154 (2013) 3796–3806, https://doi.org/10.1210/en.2013-1167.
[16] M. Mariotti, P.G. Ridge, Y. Zhang, A.V. Lobanov, T.H. Pringle, R. Guigo, D. L. Hatfield, V.N. Gladyshev, Composition and evolution of the vertebrate and mammalian selenoproteomes, PloS One 7 (2012), e33066, https://doi.org/10.1371/journal.pone.0033066.
[17] G.V. Kryukov, S. Castellano, S.V. Novoselov, A.V. Lobanov, O. Zehtab, R. Guigó, V.N. Gladyshev, Characterization of mammalian selenoproteomes, Science 300 (2003) 1439–1443, https://doi.org/10.1126/science.1083516.
[18] L.L. Chen, J.Q. Huang, Y. Xiao, Y.Y. Wu, F.Z. Ren, X.G. Lei, Knockout of selenoprotein V affects regulation of selenoprotein expression by dietary selenium and fat intakes in mice, J. Nutr. 150 (2020) 483–491, https://doi.org/10.1093/jn/nxz287.
[19] X. Zhang, W. Xiong, L.-L. Chen, J.-Q. Huang, X.G. Lei, Selenoprotein V protects against endoplasmic reticulum stress and oxidative injury induced by pro-oxidants, Free Radical Biol. Med. 160 (2020) 670–679, https://doi.org/10.1016/j.freeradbiomed.2020.08.011.
[20] B. Hou, J. Zhou, C. Gong, Y. Xu, X. Liu, Y. Zhong, X. Shen, Effects of RNA interference to selenoprotein V gene on cytobiological behaviors in human malignant melanoma A375 cells, Acta Nutr. Sin. 36 (2014) 612–618.
[21] E.G. Varlamova, S.V. Novoselov, V.I. Novoselov, cDNA cloning and the expression and determination of substrate specificity of mice selenocysteine-containing protein SelV (Selenoprotein V), Mol. Biol. 49 (2015) 700–704, https://doi.org/10.1134/s0026893315050180.
[22] M.V. Goltyaev, E.G. Varlamova, V.I. Novoselov, E.E. Fesenko, Determination of mgpx6 and mselv gene mRNA expression during mouse postnatal development, Dokl. Biochem. Biophys. 457 (2014) 132–133, https://doi.org/10.1134/S1607672914040048.
[23] E.G. Varlamova, V.I. Novolelov, Search for partners of a new mammalian selenium-containing SelV and expression of its mRNA, Mol. Biol. 46 (2012) 276–284, https://doi.org/10.1134/S0026893312010244.
[24] H. Zhao, K. Li, J.Y. Tang, J.C. Zhou, K.N. Wang, X.J. Xia, X.G. Lei, Expression of selenoprotein genes is affected by obesity of pigs fed a high-fat diet, J. Nutr. 145 (2015) 1394–1401, https://doi.org/10.3945/jn.115.211318.
[25] G. Frühbeck, S. Becerril, N. Sáinz, P. Garrastachu, M.J. García-Velloso, BAT: a new target for human obesity? Trends Pharmacol. Sci. 30 (2009) 387–396, https://doi.org/10.1016/j.tips.2009.05.003.
[26] B.M. Spiegelman, J.S. Flier, Obesity and the regulation of energy balance, Cell 104 (2001) 531–543, https://doi.org/10.1016/S0092-8674(01)00240-9.
[27] R. Oelkrug, E.T. Polymeropoulos, M. Jastroch, Brown adipose tissue: physiological function and evolutionary significance, J. Comp. Physiol. B. 185 (2015) 587–606, https://doi.org/10.1007/s00360-015-0907-7.
[28] A.P. Beigneux, C.M. Allan, N.P. Sandoval, G.W. Cho, P.J. Heizer, R.S. Jung, K. L. Stanhope, P.J. Havel, G. Birrane, M. Meiyappan, J.E. Gill, M. Murakami, K. Miyashita, K. Nakajima, M. Ploug, L.G. Fong, S.G. Young, Lipoprotein lipase is active as a monomer, Proc. Natl. Acad. Sci. U.S.A. 116 (2019) 6319–6328, https://doi.org/10.1073/pnas.1900983116.

[29] F. Ameer, L. Scandiuzzi, S. Hasnain, H. Kalbacher, N. Zaidi, De novo lipogenesis in health and disease, Metab. Clin. Exp. 63 (2014) 895–902, https://doi.org/10.1016/j.metabol.2014.04.003.

[30] R. Zimmermann, J.G. Strauss, G. Haemmerle, G. Schoiswohl, R. Birner-Gruenberger, M. Riederer, A. Lass, G. Neuberger, F. Eisenhaber, A. Hermetter, R. Zechner, Fat mobilization in adipose tissue is promoted by adipose triglyceride lipase, Science 306 (2004) 1383–1386, https://doi.org/10.1126/science.1100747.

[31] R. Zechner, R. Zimmermann, T.O. Eichmann, S.D. Kohlwein, G. Haemmerle, A. Lass, F. Madeo, FAT SIGNALS–lipases and lipolysis in lipid metabolism and signaling, Cell Metabol. 15 (2012) 279–291, https://doi.org/10.1016/j.cmet.2011.12.018.

[32] J.-P. Bonnefont, F. Djouadi, C. Prip-Buus, S. Gobin, A. Munnich, J. Bastin, Carnitine palmitoyltransferases 1 and 2: biochemical, molecular and medical aspects, Mol. Aspect. Med. 25 (2004) 495–520, https://doi.org/10.1016/j.mam.2004.06.004.

[33] H. Ohno, K. Shinoda, B.M. Spiegelman, S. Kajimura, PPAR gamma agonists induce a white-to-brown fat conversion through stabilization of PRDM16 protein, Cell Metabol. 15 (2012) 395–404, https://doi.org/10.1016/j.cmet.2012.01.019.

[34] P. Seale, B. Bjork, W. Yang, S. Kajimura, S. Chin, S. Kuang, A. Scime, S. Devarakonda, H.M. Conroe, H. Erdjument-Bromage, P. Tempst, M.A. Rudnicki, D.R. Beier, B.M. Spiegelman, PRDM16 controls a brown fat/skeletal muscle switch, Nature 454 (2008) 961–967, https://doi.org/10.1038/nature07182.

[35] B. Cannon, J. Nedergaard, Brown adipose tissue function and physiological significance, Physiol. Rev. 84 (2004) 277–359, https://doi.org/10.1152/physrev.00015.2003.

[36] X.X. Yuan, G. Wei, Y.L. You, Y.Y. Huang, H.J. Lee, M. Dong, J. Lin, T. Hu, H. L. Zhang, C.H. Zhang, H.Q. Zhou, R.C. Ye, X.L. Qi, B.Q. Zhai, W.D. Huang, S. N. Liu, W. Xie, Q.S. Liu, X.M. Liu, C.B. Cui, D.H. Li, J.C. Zhan, J. Cheng, Z. Q. Yuan, W.Z. Jin, Rutin ameliorates obesity through brown fat activation, Faseb. J. 31 (2017) 333–345, https://doi.org/10.1096/fj.201600459RR.

[37] Adipose expression of tumor necrosisi-factor-alpha-direct role in obesity-linked insulin resistance, Science 259 (1993) 87–91, https://doi.org/10.1126/science.7678183.

[38] H. Xu, G.T. Barnes, Q. Yang, G. Tan, D. Yang, C.J. Chou, J. Sole, A. Nichols, J. S. Ross, L.A. Tartaglia, H. Chen, Chronic inflammation in fat plays a crucial role in the development of obesity-related insulin resistance, J. Clin. Invest. 112 (2003) 1821–1830, https://doi.org/10.1172/jci200319451.

[39] P. Sartipy, D.J. Loskutoff, Monocyte chemoattractant protein 1 in obesity and insulin resistance, Proc. Natl. Acad. Sci. U.S.A. 100 (2003) 7265–7270, https://doi.org/10.1073/pnas.1133870100.

[40] D.G. Hardie, F.A. Ross, S.A. Hawley, AMPK: a nutrient and energy sensor that maintains energy homeostasis, Nat. Rev. Mol. Cell Biol. 13 (2012) 251–262, https://doi.org/10.1038/nrm3311.

[41] E. Hondares, M. Rosell, J. Diaz-Delfin, Y. Olmos, M. Monsalve, R. Iglesias, F. Villarroya, M. Giralt, Peroxisome proliferator-activated receptor alpha (PPARalpha) induces PPARgamma coactivator 1alpha (PGC-1alpha) gene expression and contributes to thermogenic activation of brown fat: involvement of PRDM16, J. Biol. Chem. 286 (2011) 43112–43122, https://doi.org/10.1074/jbc.M111.252775.

[42] S.J. Kim, T.Y. Tang, M. Abbott, J.A. Viscarra, Y.H. Wang, H.S. Sul, AMPK phosphorylates desnutrin/ATGL and hormone-sensitive lipase to regulate lipolysis and fatty acid oxidation within adipose tissue, Mol. Cell Biol. 36 (2016) 1961–1976, https://doi.org/10.1128/mcb.00244-16.

[43] S. Zhong, L. Li, Y.L. Zhang, L. Zhang, J. Lu, S. Guo, N. Liang, J. Ge, M. Zhu, Y. Tao, Acetaldehyde dehydrogenase 2 interactions with LDLR and AMPK regulate foam cell formation, J. Clin. Invest. 129 (2019) 252–267, https://doi.org/10.1172/JCI122064.

[44] S.A. Hawley, D. Pan, K.J. Mustard, L. Ross, J. Bain, A.M. Edelman, B. G. Frenguelli, D.G. Hardie, Calmodulin-dependent protein kinase kinase-beta is an alternative upstream kinase for AMP-activated protein kinase, Cell Metabol. 2 (2005) 9–19, https://doi.org/10.1016/j.cmet.2005.05.009.

[45] S.A. Hawley, J. Boudeau, J.L. Reid, K.J. Mustard, H.D. Grahame, Complexes between the LKB1 tumor suppressor, STRADα/β and MO25α/β are upstream kinases in the AMP-activated protein kinase cascade, J. Biol. 2 (2003) 28, https://doi.org/10.1186/1475-4924- 2-28.

[46] J.W. Bullen, J.L. Balsbaugh, D. Chanda, J. Shabanowitz, D.F. Hunt, D. Neumann, G.W. Hart, Cross-talk between two essential nutrient-sensitive enzymes: O-GlcNAc transferase (OGT) and AMP-activated protein kinase (AMPK), J. Biol. Chem. 289 (2014) 10592–10606, https://doi.org/10.1074/jbc.M113.523068.

[47] B. Luo, G.J. Parker, R.C. Cooksey, Y. Soesanto, M. Evans, D. Jones, D.A. Mcclain, Chronic hexosamine flux stimulates fatty acid oxidation by activating AMP-activated protein kinase in adipocytes, J. Biol. Chem. 282 (2007) 7172–7180, https://doi.org/10.1074/jbc.M607362200.

[48] R. Gélinas, J. Dontaine, S. Horman, C. Beauloye, L. Bultot, L. Bertrand, AMP-activated protein kinase and O-GlcNAcylation, two partners tightly connected to regulate key cellular processes, Front. Endocrinol. 9 (2018) 519, https://doi.org/10.3389/fendo.2018.00519.

[49] Q.R. Xu, C.H. Yang, Y. Du, Y.L. Chen, H.L. Liu, M. Deng, H.X. Zhang, L. Zhang, T. Z. Liu, Q.G. Liu, L.W. Wang, Z.K. Lou, H.D. Pei, AMPK regulates histone H2B O-GlcNAcylation, Nucleic Acids Res. 42 (2014) 5594–5604, https://doi.org/10.1093/nar/gku236.

[50] P.J. Fernandez-Marcos, J. Auwerx, Regulation of PGC-1 alpha, a nodal regulator of mitochondrial biogenesis, Am. J. Clin. Nutr. 93 (2011) 884S–890S, https://doi.org/10.3945/ajcn.110.001917.

[51] L.J. Watson, H.T. Facundo, G.A. Ngoh, M. Ameen, R.E. Brainard, K.M. Lemma, B. W. Long, S.D. Prabhu, Y.-T. Xuan, S.P. Jones, O-linked β-acetylglucosamine transferase is indispensable in the failing heart, Proc. Natl. Acad. Sci. U.S.A. 107 (2010) 17797–17802, https://doi.org/10.1073/pnas.1001907107.

[52] E.G. Varlamova, Intracellular localization of mammalian selenoproteins SelV (selenoprotein V) and Gpx 6 (glutathione peroxidase 6), Fundament 9 (2011) 326–330, https://doi.org/10.1134/s0026893312050111.

[53] J.-C. Zhou, H. Zhao, J.-G. Li, X.-J. Xia, K.-N. Wang, Y.-J. Zhang, Y. Liu, Y. Zhao, X. G. Lei, Selenoprotein gene expression in thyroid and pituitary of young pigs is not affected by dietary selenium deficiency or excess, J. Nutr. 139 (2009) 1061–1066, https://doi.org/10.3945/jn.109.104901.

[54] J.Q. Huang, F.Z. Ren, Y.Y. Jiang, C. Xiao, X.G. Lei, Selenoproteins protect against avian nutritional muscular dystrophy by metabolizing peroxides and regulating redox/apoptotic signaling, Free Radical Biol. Med. 83 (2015) 129–138, https://doi.org/10.1016/j.freeradbiomed.2015.01.033.

[55] A.M. Cancel, D. Lobdell, P. Mendola, S.D. Perreault, Objective evaluation of hyperactivated motility in rat spermatozoa using computer-assisted sperm analysis, Hum. Reprod. 15 (2000) 1322–1328, https://doi.org/10.1093/humrep/15.6.1322.

[56] B. Prunet-Marcassus, B. Cousin, D. Caton, M. André, L. Pénicaud, L. Casteilla, From heterogeneity to plasticity in adipose tissues: site-specific differences, Exp. Cell Res. 312 (2006) 727–736, https://doi.org/10.1016/j.yexcr.2005.11.021.

[57] J.Z. Long, K.J. Svensson, L.A. Bateman, H. Lin, T. Kamenecka, I.A. Lokurkar, J. Lou, R.R. Rao, M.R. Chang, M.P. Jedrychowski, J.A. Paulo, S.P. Gygi, P. R. Griffin, D.K. Nomura, B.M. Spiegelman, The secreted enzyme PM20D1 regulates lipidated amino acid uncouplers of mitochondria, Cell 166 (2016) 424–435, https://doi.org/10.1016/j.cell.2016.05.071.

[58] Y. Akakabe, M. Koide, Y. Kitamura, K. Matsuo, T. Ueyama, S. Matoba, H. Yamada, K. Miyata, Y. Oike, K. Ikeda, Ecscr regulates insulin sensitivity and predisposition to obesity by modulating endothelial cell functions, Nat. Commun. 4 (2013) 2389–2401, https://doi.org/10.1038/ncomms3389.

[59] H. Shi, A. Munk, T.S. Nielsen, M.R. Daughtry, L. Larsson, S. Li, K.F. Hoyer, H. W. Geisler, K. Sulek, R. Kjobsted, T. Fisher, M.M. Andersen, Z. Shen, U.K. Hansen, E.M. England, Z. Cheng, K. Hojlund, J.F.P. Wojtaszewski, X. Yang, M.W. Hulver, R.F. Helm, J.T. Treebak, D.E. Gerrard, Skeletal muscle O-GlcNAc transferase is important for muscle energy homeostasis and whole-body insulin sensitivity, Mol. Metab. 11 (2018) 160–177, https://doi.org/10.1016/j.molmet.2018.02.010.

[60] J. Vandesompele, K. De Preter, F. Pattyn, B. Poppe, N. Van Roy, A. De Paepe, F. Speleman, Accurate normalization of real-time quantitative RT-PCR data by geometric averaging of multiple internal control genes, Genome Biol. 3 (2002) 34.1–34.12. https://10.1186/gb-2002-3-7-research0034.

[61] L. Yu, Y. Wang, S. Huang, J.J. Wang, Z.Q. Deng, Q. Zhang, W. Wu, X.L. Zhang, Z. Liu, W.M. Gong, Z.Z. Chen, Structural insights into a novel histone demethylase PHF8, Cell Res. 20 (2010) 166–173, https://doi.org/10.1038/cr.2010.8.

[62] S.P. Yang, G.L. Bai, L.L. Chen, Q. Shen, X.M. Diao, G.H. Zhao, The interaction of phenolic acids with Fe(III) in the presence of citrate as studied by isothermal titration calorimetry, Food Chem. 157 (2014) 302–309, https://doi.org/10.1016/j.foodchem.2014.02.052.

[63] J.K. Yang, W. Xiong, F.Y. Chen, L. Xu, Z.G. Han, Aromatic amino acids in the cellulose binding domain of Penicillium crustosum endoglucanase EGL1 differentially contribute to the cellulose affinity of the enzyme, PloS One 12 (2017), e0176444, https://doi.org/10.1371/journal.pone.0176444.

[64] S.V. Novoselov, A.V. Lobanov, D. Hua, M.V. Kasaikina, D.L. Hatfield, V. N. Gladyshev, A highly efficient form of the selenocysteine insertion sequence element in protozoan parasites and its use in mammalian cells, Proc. Natl. Acad. Sci. U.S.A. 104 (2007) 7857–7862, https://doi.org/10.1073/pnas.0610683104.

[65] H.-B. Ruan, X. Han, M.-D. Li, Jay p. Singh, K. Qian, S. Azarhoush, L. Zhao, Anton m. Bennett, Varman t. Samuel, J. Wu, John r. Yates, X. Yang, O-GlcNAc transferase/host cell factor c1 complex regulates gluconeogenesis by modulating PGC-1α stability, Cell Metabol. 16 (2012) 226–237, https://doi.org/10.1016/j.cmet.2012.07.006.

[66] M.C. Medina, J. Molina, Y. Gadea, A. Fachado, M. Murillo, G. Simovic, A. Pileggi, A. Hernández, H. Edlund, A.C. Bianco, The thyroid hormone-inactivating type III deiodinase is expressed in mouse and human β-cells and its targeted inactivation impairs insulin secretion, Endocrinology 152 (2011) 3717–3727, https://doi.org/10.1210/en.2011- 1210.

[67] S.C. Schriever, A. Zimprich, K. Pfuhlmann, P. Baumann, F. Giesert, V. Klaus, D. G. Kabra, U. Hafen, A. Romanov, M.H. Tschöp, W. Wurst, M. Conrad, S.M. Hölter, D. Vogt Weisenhorn, P.T. Pfluger, Alterations in neuronal control of body weight and anxiety behavior by glutathione peroxidase 4 deficiency, Neuroscience 357 (2017) 241–254, https://doi.org/10.1016/j.neuroscience.2017.05.050.

[68] Z.F. Wu, M.E. Martinez, D.L.S. Germain, A. Hernandez, Type 3 deiodinase role on central thyroid hormone action affects the leptin-melanocortin system and circadian activity, Endocrinology 158 (2017) 419–430, https://doi.org/10.1210/en.2016-1680.

[69] X. Zheng, B. Ren, X. Li, H. Yan, Q. Xie, H. Liu, J. Zhou, J. Tian, K. Huang, Selenoprotein F knockout leads to glucose and lipid metabolism disorders in mice, J. Biol. Inorg. Chem. 25 (2020) 1009–1022, https://doi.org/10.1007/s00775-020-01821-z.

[70] S.V. Iverson, S. Eriksson, J. Xu, J.R. Prigge, E.A. Talago, T.A. Meade, E.S. Meade, M.R. Capecchi, E.S.J. Arnér, E.E. Schmidt, A Txnrd1-dependent metabolic switch alters hepatic lipogenesis, glycogen storage, and detoxification, Free Radical Biol. Med. 63 (2013) 369–380, https://doi.org/10.1016/j.freeradbiomed.2013.05.028.

[71] J.C. Avery, Y. Yamazaki, F.W. Hoffmann, B. Folgelgren, P.R. Hoffmann, Selenoprotein I is essential for murine embryogenesis, Arch. Biochem. Biophys. 689 (2020) 5, https://doi.org/10.1016/j.abb.2020.108444.
[72] J.-Y. Heo, H.-N. Cha, K.Y. Kim, E. Lee, S.-J. Kim, Y.-W. Kim, J.-Y. Kim, I.-K. Lee, V. N. Gladyshev, H.-Y. Kim, S.-Y. Park, Methionine sulfoxide reductase B1 deficiency does not increase high-fat diet-induced insulin resistance in mice, Free Radic. Res. 51 (2017) 24–37, https://doi.org/10.1080/10715762.2016.1261133.
[73] M. Conrad, C. Jakupoglu, S.G. Moreno, S. Lippl, A. Banjac, M. Schneider, H. Beck, A.K. Hatzopoulos, U. Just, F. Sinowatz, Essential role for mitochondrial thioredoxin reductase in hematopoiesis, heart development, and heart function, Mol. Cell Biol. 24 (2004) 9414–9423, https://doi.org/10.1128/MCB.24.21.9414-9423.2004.
[74] C. Perrine, A.T. Bertrand, B. Maud, F. Arnaud, L.G. Fabien, C. Marie, C. Guillaume, R. Mathieu, K. Alain, L. Alain, Satellite cell loss and impaired muscle regeneration in selenoprotein N deficiency, Hum. Mol. Genet. (2011) 694–704, https://doi.org/10.1093/hmg/ddq515.
[75] C.W. Barrett, W. Ning, X. Chen, J.J. Smith, M.K. Washington, K.E. Hill, L. A. Coburn, R.M. Peek, R. Chaturvedi, K.T. Wilson, R.F. Burk, C.S. Williams, Tumor suppressor function of the plasma glutathione peroxidase Gpx3 in colitis-associated carcinoma, Canc. Res. 73 (2013) 1245–1255, https://doi.org/10.1158/0008-5472.can-12-3150.
[76] J. Liu, A. Hernandez-Ono, M.J. Graham, V.A. Galton, H.N. Ginsberg, Type 1 deiodinase regulates ApoA-I gene expression and ApoA-I synthesis independent of thyroid hormone signaling, Atertio. Thromb. Vasc. Biol. 36 (2016) 1356–1366, https://doi.org/10.1161/ATVBAHA.116.307330.
[77] R.L. Norton, G.J. Fredericks, Z. Huang, J.D. Fay, F.W. Hoffmann, P.R. Hoffmann, Selenoprotein K regulation of palmitoylation and calpain cleavage of ASAP2 is required for efficient Fc gamma R-mediated phagocytosis, J. Leukoc. Biol. 101 (2017) 439–448, https://doi.org/10.1189/jlb.2A0316-156RR.
[78] C. Lennicke, J. Rahn, C. Wickenhauser, R. Lichtenfels, A.S. Muller, L. A. Wessjohann, A.P. Kipp, B. Seliger, Loss of epithelium-specific GPx 2 results in aberrant cell fate decisions during intestinal differentiation, Oncotarget 9 (2018) 539–552, https://doi.org/10.18632/oncotarget.22640.
[79] A.B. Addinsall, C.R. Wright, T.L. Kotsiakos, Z.M. Smith, T.R. Cook, S. Andrikopoulos, C. Van Der Poel, N. Stupka, Impaired exercise performance is independent of inflammation and cellular stress following genetic reduction or deletion of selenoprotein S, Am. J. Physiol. Regul. Integr. Comp. Physiol. 318 (2020) R981–R996, https://doi.org/10.1152/ajpregu.00321.2019.
[80] Z. Song, A. Xiaoli, F. Yang, Regulation and metabolic significance of de novo lipogenesis in adipose tissues, Nutrients 10 (2018) 1383–1404, https://doi.org/10.3390/nu10101383.
[81] P.H. Weinstock, S. Levakfrank, L.C. Hudgins, H. Radner, J.M. Friedman, R. Zechner, J.L. Breslow, Lipoprotein lipase controls fatty acid entry into adipose tissue, but fat mass is preserved by endogenous synthesis in mice deficient in adipose tissue lipoprotein lipase, Proc. Natl. Acad. Sci. U.S.A. 94 (1997) 10261–10266, https://doi.org/10.1073/pnas.94.19.10261.
[82] M.H. Jang, N.H. Kang, S. Mukherjee, J.W. Yun, Theobromine, a methylxanthine in cocoa bean, stimulates thermogenesis by inducing white fat browning and activating brown adipocytes, Biotechnol. Bioproc. Eng. 23 (2018) 617–626, https://doi.org/10.1007/s12257-018-0434-y.
[83] F.F. Zhu, Y.M. Wang, G.Z. He, Y.F. Chen, Y.D. Gao, Different effects of acetyl-CoA carboxylase inhibitor TOFA on airway inflammation and airway resistance in a mice model of asthma, Pharmacol. Rep. 72 (2020) 1011–1020, https://doi.org/10.1007/s43440-019- 00027-8.
[84] X. Yan, M.P. Pepper, M.Z. Vatamaniuk, C.A. Roneker, L. Li, X.G. Lei, Dietary selenium deficiency partially rescues type 2 diabetes-like phenotypes of glutathione peroxidase-1-overexpressing male mice, J. Nutr. 142 (2012) 1975–1982, https://doi.org/10.3945/jn.112.164764.
[85] A. Marsili, C. Aguayo-Mazzucato, T. Chen, A. Kumar, M. Chung, E.P. Lunsford, J. W. Harney, V.T. Thuy, E. Gianetti, W. Ramadan, C. Chou, S. Bonner-Weir, P. R. Larsen, J.E. Silva, A.M. Zavacki, Mice with a targeted deletion of the type 2 deiodinase are insulin resistant and susceptible to diet induced obesity, PloS One 6 (2011), e20832, https://doi.org/10.1371/journal.pone.0020832.
[86] M.R. Bond, J.A. Hanover, O-GlcNAc cycling: a link between metabolism and chronic disease, in: R.J. Cousins (Ed.), Annu. Rev. Nutr. 33 (2013) 205–229, https://doi.org/10.1146/annurev-nutr-071812-161240. Annual Reviews, Palo Alto.
[87] K.R. Harwood, J.A. Hanover, Nutrient-driven O-GlcNAc cycling – think globally but act locally, J. Cell Sci. 127 (2014) 1857–1867, https://doi.org/10.1242/jcs.113233.
[88] C.M. Ferrer, V.L. Sodi, M.J. Reginato, O-GlcNAcylation in cancer biology: linking metabolism and signaling, J. Mol. Biol. 428 (2016) 3282–3294, https://doi.org/10.1016/j.jmb.2016.05.028.
[89] V.L. Sodi, Z.A. Bacigalupa, C.M. Ferrer, J.V. Lee, W.A. Gocal, D. Mukhopadhyay, K.E. Wellen, M. Ivan, M.J. Reginato, Nutrient sensor O-GlcNAc transferase controls cancer lipid metabolism via SREBP-1 regulation, Oncogene 37 (2018) 924–934, https://doi.org/10.1038/onc.2017.395.
[90] T. Gong, A.C. Hashimoto, A.R. Sasuclark, V.S. Khadka, A. Gurary, M.W. Pitts, Selenoprotein M promotes hypothalamic leptin signaling and thioredoxin antioxidant activity, Antioxidants Redox Signal. (2019) 1–13, https://doi.org/10.1089/ars.2018.7594, 00.
[91] H. Misu, H. Takayama, Y. Saito, Y. Mita, A. Kikuchi, K. Ishii, K. Chikamoto, T. Kanamori, N. Tajima, F. Lan, Y. Takeshita, M. Honda, M. Tanaka, S. Kato, N. Matsuyama, Y. Yoshioka, K. Iwayama, K. Tokuyama, N. Akazawa, S. Maeda, K. Takekoshi, S. Matsugo, N. Noguchi, S. Kaneko, T. Takamura, Deficiency of the hepatokine selenoprotein P increases responsiveness to exercise in mice through upregulation of reactive oxygen species and AMP-activated protein kinase in muscle, Nat. Med. 23 (2017) 508–519, https://doi.org/10.1038/nm.4295.
[92] V. Champattanachai, R.B. Marchase, J.C. Chatham, Glucosamine protects neonatal cardiomyocytes from ischemia-reperfusion injury via increased protein-associated OGlcNAc, Am. J. Physiol. Cell Physiol. 292 (2007) C178–C187, https://doi.org/10.1152/ajpcell.00162.2006.
[93] H. Nie, W. Yi, O-GlcNAcylation, a sweet link to the pathology of diseases, J. Zhejiang Univ. - Sci.B. 20 (2019) 437–448, https://doi.org/10.1631/jzus.B1900150.
[94] H.B. Ruan, M.O. Dietrich, Z.W. Liu, M.R. Zimmer, M.D. Li, J.P. Singh, K. Zhang, R. Yin, J. Wu, T.L. Horvath, X. Yang, O-GlcNAc transferase enables AgRP neurons to suppress browning of white fat, Cell 159 (2014) 306–317, https://doi.org/10.1016/j.cell.2014.09.010.
[95] W.D. Cheung, G.W. Hart, AMP-activated protein kinase and p38 MAPK activate O-GlcNAcylation of neuronal proteins during glucose deprivation, J. Biol. Chem. 283 (2008) 13009–13020, https://doi.org/10.1074/jbc.M801222200.
[96] W.D. Cheung, K. Sakabe, M.P. Housley, W.B. Dias, G.W. Hart, O-linked beta-Nacetylglucosaminyltransferase substrate specificity is regulated by myosin phosphatase targeting and other interacting proteins, J. Biol. Chem. 283 (2008) 33935–33941, https://doi.org/10.1074/jbc.M806199200.
[97] T.R. Whisenhunt, X.Y. Yang, D.B. Bowe, A.J. Paterson, B.A. Van Tine, J. E. Kudlow, Disrupting the enzyme complex regulating O-GlcNAcylation blocks signaling and development, Glycobiology 16 (2006) 551–563, https://doi.org/10.1093/glycob/cwj096.
[98] S. Bijland, S.J. Mancini, I.P. Salt, Role of AMP-activated protein kinase in adipose tissue metabolism and inflammation, Clin. Sci. 124 (2013) 491–507, https://doi.org/10.1042/cs20120536.
[99] R. Lage, C. Diéguez, A. Vidal-Puig, M. López, AMPK: a metabolic gauge regulating whole-body energy homeostasis, Trends Mol. Med. 14 (2008) 539–549, https://doi.org/10.1016/j.molmed.2008.09.007.
[100] S.A. Hawley, D.A. Pan, K.J. Mustard, L. Ross, J. Bain, A.M. Edelman, B. G. Frenguelli, D.G. Hardie, Calmodulin-dependent protein kinase kinase-beta is an alternative upstream kinase for AMP-activated protein kinase, Cell Metabol. 2 (2005) 9–19, https://doi.org/10.1016/j.cmet.2005.05.009.
[101] A. Woods, K. Dickerson, R. Heath, S.P. Hong, M. Momcilovic, S.R. Johnstone, M. Carlson, D. Carling, Ca2+/calmodulin-dependent protein kinase kinase-beta acts upstream of AMP-activated protein kinase in mammalian cells, Cell Metabol. 2 (2005) 21–33, https://doi.org/10.1016/j.cmet.2005.06.005.
[102] D. Vigetti, M. Viola, E. Karousou, G. De Luca, A. Passi, Metabolic control of hyaluronan synthases, Matrix Biol. 35 (2014) 8–13, https://doi.org/10.1016/j.matbio.2013.10.002.
[103] T. Wang, Q.J. Yu, J.J. Li, B. Hu, Q. Zhao, C.M. Ma, W.H. Huang, L.G. Zhuo, H. Q. Fang, L.J. Liao, Y.E. Chin, Y.H. Jiang, O-GlcNAcylation of fumarase maintains tumour growth under glucose deficiency, Nat. Cell Biol. 19 (2017) 833–843, https://doi.org/10.1038/ncb3562.
[104] H. Imai, F. Hirao, T. Sakamoto, K. Sekine, Y. Mizukura, M. Saito, T. Kitamoto, M. Hayasaka, K. Hanaoka, Y. Nakagawa, Early embryonic lethality caused by targeted disruption of the mouse PHGPx gene, Biochem. Biophys. Res. Commun. 305 (2003) 278–286, https://doi.org/10.1016/S0006-291X(03)00734-4.
[105] H. Imai, N. Hakkaku, R. Iwamoto, J. Suzuki, T. Suzuki, Y. Tajima, K. Konishi, S. Minami, S. Ichinose, K. Ishizaka, S. Shioda, S. Arata, M. Nishimura, S. Naito, Y. Nakagawa, Depletion of selenoprotein GPx4 in spermatocytes causes male infertility in mice, J. Biol. Chem. 284 (2009) 32522–32532, https://doi.org/10.1074/jbc.M109.016139.
[106] I. Ingold, M. Aichler, E. Yefremova, A. Roveri, K. Buday, S. Doll, A. Tasdemir, N. Hoffard, W. Wurst, A. Walch, F. Ursini, J.P. Friedmann Angeli, M. Conrad, Expression of a catalytically inactive mutant form of glutathione peroxidase 4 (Gpx4) confers a dominantnegative effect in male fertility, J. Biol. Chem. 290 (2015) 14668–14678, https://doi.org/10.1074/jbc.M115.656363.
[107] L.A. Katunga, P. Gudimella, J.T. Efird, S. Abernathy, T.A. Mattox, C. Beatty, T. M. Darden, K.A. Thayne, H. Alwair, A.P. Kypson, J.A. Virag, E.J. Anderson, Obesity in a model of gpx4 haploinsufficiency uncovers a causal role for lipid-derived aldehydes in human metabolic disease and cardiomyopathy, Mol. Metab. 4 (2015) 493–506, https://doi.org/10.1016/j.molmet.2015.04.001.